A Membrane Biosensor for the Detection of Lactate in Body Fluids

by

Yuxing Wang

A thesis

presented to the University of Waterloo

in fulfillment of the

thesis requirement for the degree of

Master of Science

in

Chemistry (Nanotechnology)

Waterloo, Ontario, Canada, 2019

AUTHOR'S DECLARATION

I hereby declare that I am the sole author of this thesis. This is a true copy of the thesis, including any required final revisions, as accepted by my examiners.

I understand that my thesis may be made electronically available to the public.

Abstract

The increased demand of real-time and convenient heath monitoring has spurned the rapid development of wearable health monitoring devices. In these devices, the central part is the sensor that can convert health information into readable data. Biosensors have been widely used in this field since they can be easily fit into small devices and provide sensitive and selective detections of key health indicators in the human body.

In this study, we developed a membrane biosensor used to detect lactate. Lactate is a significant health indicator. The variations of the lactate level in the human body imply physiological changes, such as indicating decubitus ulcers for bedridden people. Our membrane biosensor is formed on thin-film gold electrodes. Its working electrode, on which lactate oxidase is immobilized, generates a current signal that is related to the lactate concentration of the electrolyte solution. The sensor also has a built-in solid-state Ag/AgCl electrode that is capable of maintaining a stable potential for hours. The membrane biosensor was able to generate reliable and stable signals. Its dynamic detection range was 4 to 30 mM, with a detection limit higher than the highest physiological lactate level. To mimic the real working scenario for the membrane sensor, it was attached to a transdermal microneedle patch and placed inside a sensor-enclosing device. The microneedles are able to pierce the human skin and extract interstitial fluid and capillary blood. Body fluids including human plasma and whole blood were used to test the sensor. Experimental results revealed that the membrane sensor could provide stable and consistent signals in plasma but was unreliable in whole blood.

This master's thesis demonstrates the feasibility of using a membrane sensor with a simple configuration to detect lactate while assembled in a transdermal device, and provides fundamental knowledge for the further modifications of this membrane biosensor.

Acknowledgements

First of all, I would like to express my deepest gratitude to my supervisor, Dr. Shirley Tang, for the constant support and guidance from her during the two years of my study and research in Tang's lab.

I am also grateful to my committee members, Prof. Vivek Maheshwari and Prof. Dongqing Li for their great assistance to my MSc study.

The group members in Tang's lab offered their help to me and I would like to thank all of them. Dr. Yael Zilberman-Samkov helped me a lot in terms of using the laser cutter and fabricating the electrodes. Zhi li gave me instructions of the electrochemical workstation and provided professional assistance to me when I encountered problems. Other members, including Yun Wu, Andrew Christopher Wenger and Irfani Ausri were always there to help and support me. Our new member, Zimeng Wang, worked with me and Yael to assemble the device for blood separation.

Finally, I would like to thank my parents for supporting my overseas study.

Table of Contents

List of Figures

List of Tables

List of Abbreviations

ATP: adenosine triphosphate

BSA: bovine serum albumin

CE: counter electrode

CV: cyclic voltammetry

CV gram: cyclic voltammogram

DPV: differential pulse voltammetry

EB-PVD: electron-beam physical vapor deposition

FED: fabric-based electrochemical device

GA: glutaraldehyde

GOD: glucose oxidase

Ip: peak current

ISF: interstitial fluid

LDH: lactate dehydrogenase

LoD: limit of detection

LOD: lactate oxidase

PB: Prussian blue

PBS: phosphate-buffered saline

PDMS: polydimethylsiloxane

PMMA: poly(methyl methacrylate)

RE: reference electrode

SED: sensor-enclosing device

SSRE: solid-state reference electrode

WE: working electrode

WHMD: Wearable health monitoring device

Chapter 1. Background

1.1 Wearable Health Monitoring Devices

Nowadays, the entire world is experiencing the increasing cost of public healthcare and the aging of the population, which leads to the growing demand of personalized and distributed healthcare.[1] Various types of wearable health monitoring devices (WHMDs) are ideal personalized health monitors. Instead of going to hospitals and waiting in line, patients who use WHMDs can acquire low-cost, time-saving and real-time health monitoring (Figure 1.1).[2] During the last few years, tremendous progress has been made in the research and commercialization of WHMDs.[3,4] One typical example of the commercial WHMDs is the GlucoWatch® biographer from Cygnus, Inc. It can be worn on the wrist as a watch and monitor the blood sugar level timely.[5] Various types of WHMDs have been researched on. These smart devices could be built on clothes and contact lenses, and even directly mounted on the human skin like a tatto.[6–9]

To design and produce WHMDs, there are several basic standards to be met. For

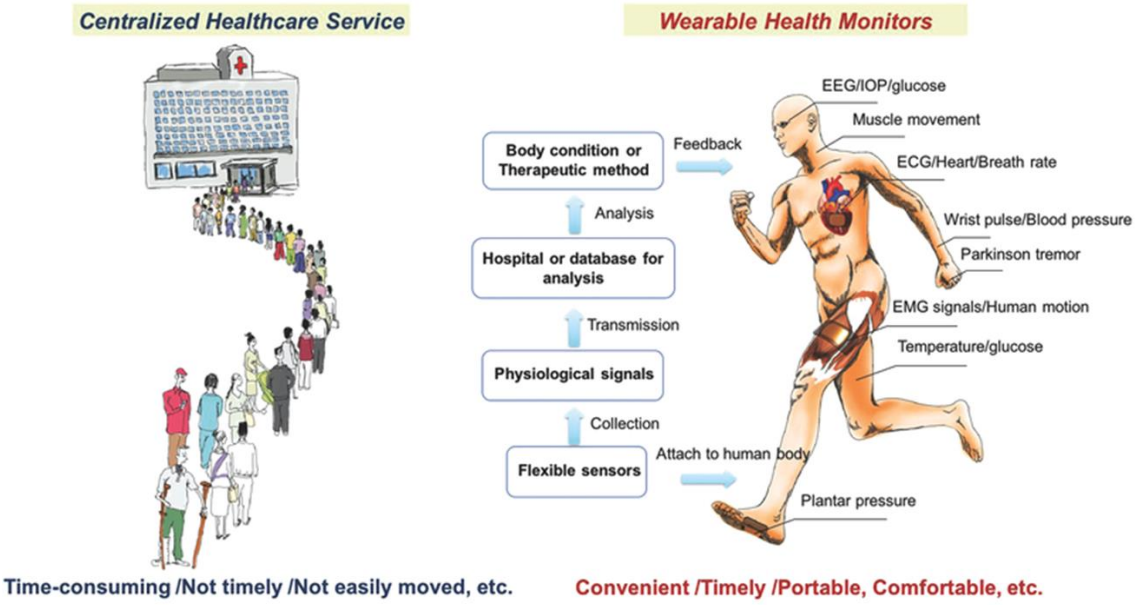

Figure 1.1. A comparison between centralized healthcare service and portable health monitors. Portable health monitors can conduct detection, data collection, signal transmission and analysis, providing feedback to the wearer in an integrated and convenient way.[2]

example, they must be lightweight and have small sizes so that they are comfortable and convenient for people to wear; the manufacturing cost of WHMDs should be low.[10] Ideally, they should be able to complete the whole process, from detecting vital health indicators to giving feedback to the users, when applied to the human body (Figure 1.1).[2] If the device is integrated with a wireless signal transmission system, the users' health information can be sent to their physicians in time.[10] With the supervision of WHMDs and physicians in daily life, it is possible that the users' physical conditions can be analyzed in more detail and those threats to users' health can be greatly avoided.

WHMDs can measure physical, chemical or biological changes of a human body, depending on the type of sensors integrated inside the devices. The sensors inside WHMDs can be divided into three types: physical sensor, chemical sensor and biosensor. Body temperature, heartbeat and respiration rate are physical properties and can be measured by piezo-resistive sensors, capacitive sensors and other physical sensors.[11] Chemicals in a human body are mainly ions, such as H^+, Na^+ and NH_4^+. Their levels can be measured by potentiometric ion-selective sensors.[12–14] To detect biological changes, such as the concentration variations of metabolites in the human body, biosensors are required and they will be further introduced in the next section. By aggregating various types of sensors in one device, one could produce a multipurpose WHMD and obtain a comprehensive view of health.[15,16]

1.2 Biosensors

The first idea of the biosensor was put forward in 1962 by Clark and Lyons.[17] They demonstrated a glucose biosensor where glucose oxidase was trapped between two Cuprophane membranes and placed on the surface of a pH electrode. When glucose molecules encounter glucose oxidase, they are converted to gluconic acid, resulting into the decrease of pH. Thus, the pH value detected by the electrode could represent the glucose concentration in solution.[17] With the wide spread of their idea, a variety of biosensors have been invented.

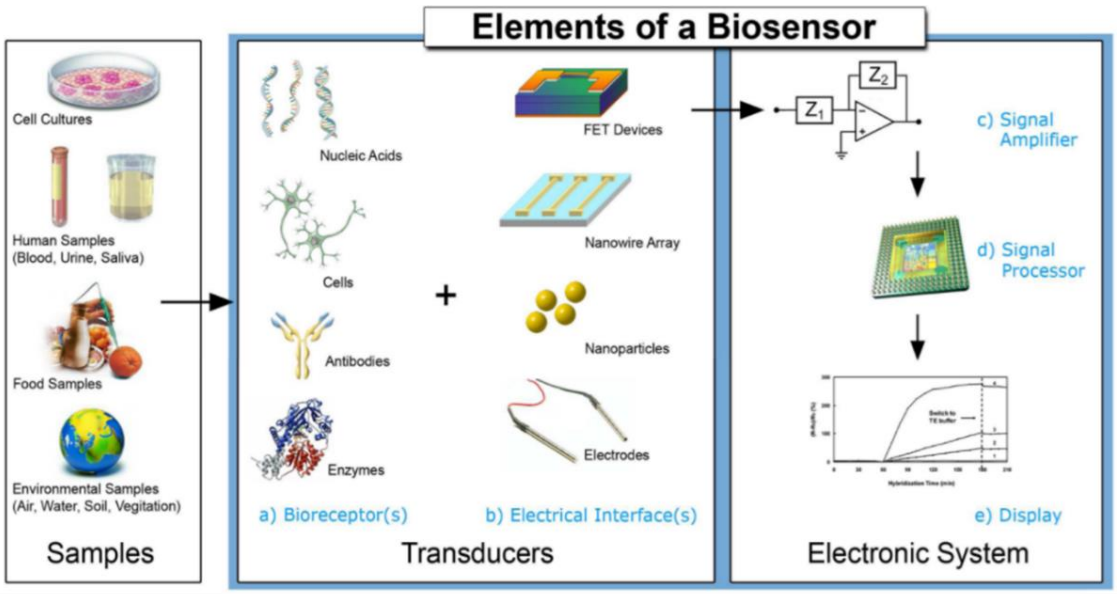

Figure 1.2. Some examples of the elements in a biosensor. A typical electrochemical biosensor is composed of a transducer and a signal processing system. The recognition elements in the transducer are biological species.[19]

Biosensors are developed from chemical sensors. A chemical sensor is typically composed of a transducer and a signal processing system. The transducer is the key component where the conversation of analyte information to displayable signals takes place. In the transducer of a chemical sensor, the recognition elements can selectively react with analytes and both of them are chemical species.[18] While in biosensors, the recognition elements are bioreceptors including nucleic acids, cells, antibodies and enzymes (Figure 1.2).[19] The high affinity between analytes and their bioreceptors, such as the base-pairing of nucleic acids, antibody-antigen interactions, and enzyme-substrate interactions, gives rise to the high selectivity and sensitivity of biosensors.[19] The interactions between the analytes and bioreceptors could result in various changes in the biosensors. Another component of the transducer, which could be potentiometric or amperometric electrodes, optoelectronic detectors or field effect transistors, captures these variations and generates relevant signals.[20] Afterwards, the signals are amplified, processed and displayed.[19]

Biosensors in WHMDs are mainly used to monitor the metabolites in the body fluids of a human, such as glucose, urea and lactate.[21–23] This work here focuses on biosensors for lactate detection.

1.3 Physiology and Clinic Significances of Lactate

Lactate has two isomers, L-(+)-lactate and D-(−)-lactate. It was confirmed by researchers that only the L-lactate form was found in mammals.[24] All lactate mentioned and used in this work is L-lactate.

Lactate is one product of glucose metabolism. Glucose is consumed in the human body to yield adenosine triphosphate (ATP) as the energy supply. Along with the release of energy, pyruvate is produced which could generate extra ATP under aerobic conditions in mitochondria.[25] However, when there is no oxygen or mitochondria, pyruvate will be converted to lactic acid by lactate dehydrogenase (LDH). At physiologic pH, most lactic acid dissociates to lactate and H^+ (Figure 1.3).[25] Just like other metabolites, lactate in a human body must be produced and consumed properly to maintain a steady state. The clearance of lactate is composed of two pathways: it can be converted back to pyruvate and glucose in the kidneys, liver and heart, or be excreted by the kidneys.[26,27]

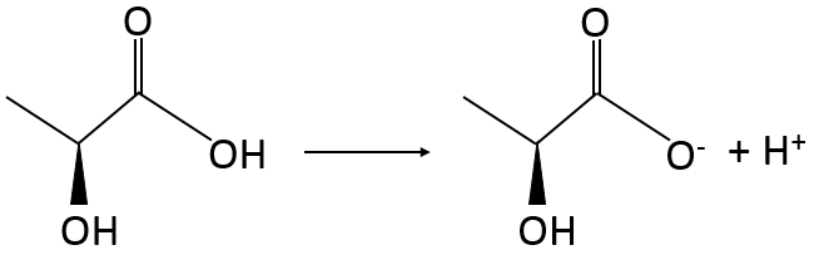

Figure 1.3. The structure of lactic acid and lactate, and the dissociation of lactic acid into lactate and hydrogen ion at physiologic pH.

The normal range of lactate in the human whole blood is 0.5 to 2.0 mM.[23] On account of physiological changes, its concentration can rise to about 18 mM.[28] The abnormal accumulation of lactate in the human body along with the decrease of blood pH is called lactic acidosis.[25] Both the over production and the reduced consumption of lactate could lead to lactic acidosis. In turn, lactic acidosis indicates that the oxygen level in the body might be abnormal, or mitochondria, the kidneys, liver and heart might not function appropriately.[25-27]

Fluctuations of lactate level can indicate certain physical conditions for both healthy and

unhealthy people. For example, the lactate level can increase significantly because of exhaustive exercise.[29] The blood lactate level has been treated as an indicator for many years to grade the endurance capability of athletes and quantify the exercise intensity.[30] For bedridden people, long-lasting high lactate level in body fluids indicates the lack of oxygen within the tissue. In such a case, the lying position of this patient must be adjusted to avoid decubitus ulcers.[29] For critical patients, the blood lactate level can be an indicator of their responses to therapies. The decline of lactate level means a greater chance to survive. According to the level variations, physicians can make adjustments to therapy strategies.[31]

To conclude, the lactate level in the human body is a significant human health indicator. As a result, timely and convenient lactate monitoring is desirable. To fulfill this requirement, nowadays, there are many household devices on the market that are designed for lactate monitoring. For example, Lactate Pro (LP, Arkray KDK, Japan) and Lactate Plus (L^+, Nova Biomedical, USA) can detect lactate in whole blood. Lactate Scout (LS, SensLab GmbH, Germany) can measure the lactate concentration from 0.5 mM to 25 mM in capillary blood. It requires a sample volume of 0.5 μL and a analysis time of 10 s.[32] The performance of these commercial portable devices has been compared to laboratory analyzers. Although these devices are reliable, their accuracies and stabilities must be improved.[32,33]

1.4 Principle of Electrochemical Lactate Detection

Many WHMDs take advantage of biosensors to detect the health markers in the human body. In terms of lactate monitoring, various electrochemical biosensors have been studied.[34–37] An electrochemical biosensor is usually a three-electrode system, consisting of a working electrode (WE), a reference electrode (RE) and a counter electrode (CE).[38] Figure 1.4 is a sketch that describes the construction of a typical three-electrode system.[39] During an electrochemical experiment, reactions take place on the WE surface, altering its potential and forming current. The CE forms a circuit with the WE to enable the current flow while measuring its value. Meanwhile, there is no current flowing through the RE and the potential of RE keeps fixed. By connecting the WE and RE with a voltmeter, the potential of WE can

be measured quantitatively.[38,39] The WE is the transducer of a biosensor and on or near its surface there are bioreceptors which can interact with the target analytes and generate corresponding electric signals.

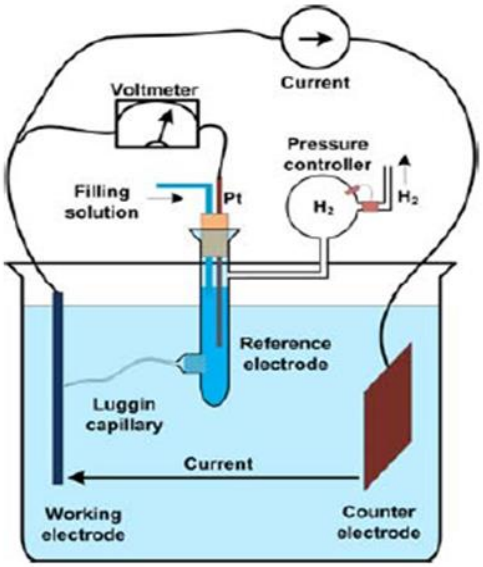

Figure 1.4. The structure of a three-electrode electrochemical cell.[39]

For lactate detection, LDH and lactate oxidase (LOD) are the most widely used bioreceptors.[40] The principles, merits and demerits of employing LDH and LOD in lactate biosensors will be introduced.

The catalytic reaction carried out by LOD is shown by the equation below:[40]

$$Lactate + O_2 \xrightarrow{LOD} Pyruvate + H_2O_2 \quad 1.1$$

Through this reaction, the detection of lactate can be converted to that of H_2O_2. The detection of H_2O_2 is based on its oxidation and reduction on an electrode surface. The redox reactions of H_2O_2 are listed below:[41]

$$\text{Oxidation: } H_2O_2 \rightarrow O_2 + 2H^+ + 2e^- \quad 1.2$$

$$\text{Reduction: } H_2O_2 + 2H^+ + 2e^- \rightarrow 2H_2O \quad 1.3$$

With more reactions proceeding, current starts to flow between the WE and CE. In cyclic voltammetry (CV), both the reduction and oxidation of H_2O_2 have corresponding peaks. The variations of H_2O_2 concentration are embodied in the changes of peak currents (I_p). Due to the

stoichiometric relationship between hydrogen peroxide and lactate, the value of I_p is proportional to the lactate concentration in the bulk solution.[23]

The catalytic reaction carried out by LDH is shown by the equation below:[40]

$$Lactate + NAD^+ \xrightarrow{LDH} Pyruvate + NADH \qquad 1.4$$

The NAD^+ and NADH are a pair of coenzymes that function as mediators to facilitate electron transfer between the electrode and LDH.[40] With more lactate molecules being consumed by LDH, more electrons will be transferred, and a larger current will be generated.

The requirement of involving additional enzymes other than LDH complicates the construction and maintenance of the biosensors, while the lactate detection with the help of LOD is a single-enzyme process.[40] However, in the biosensors based on LOD, oxygen is one of the reactants and the varying oxygen level around the electrodes can possibly bring inaccuracies to the sensors' detection.[40]

According to Rassaei *et al.*, LOD is used generally more than LDH in the research of lactate biosensors.[40] As a result, when the lactate biosensor in this work was designed, LOD was chosen to be the bioreceptor in the transducer.

1.5 Lactate Biosensors Based on LOD

Biosensors that detect lactate based on LOD can be further divided into two classes,

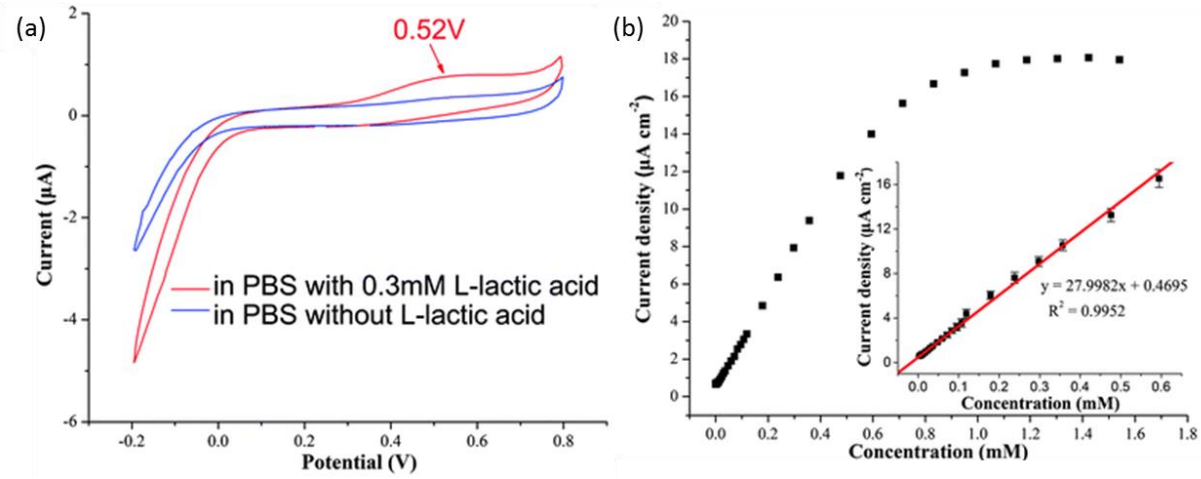

Figure 1.5. (a) CV grams of the Nafion/LOD/ZnO/Au electrode in the PBS with 0.3 mM lactate (red) and without lactate (blue). (b) The response curve of the Nafion/LOD/ZnO/Au electrode to lactate concentrations. (Inset: the linear range of the response curve).[35]

depending on whether redox mediators are incorporated or not. There are two types of redox mediators, which can facilitate the electron transfer between 1) H_2O_2 and the WE surface; 2) LOD and the WE surface.[42,43] When redox mediators exist in the biosensors, the current being recorded will not be originated from the redox reaction of H_2O_2. One example of each type of lactate biosensor will be presented in this section.

Figure 1.5 shows one example of the lactate biosensors in which no redox mediator is involved. This lactate biosensor, fabricated by Yang *et al.*, consisted of a gold WE that was modified with Nafion, ZnO nanotetrapods and LOD.[35] This Nafion/LOD/ZnO/Au electrode was tested by CV in phosphate-buffered saline (PBS) with and without lactate and the results were shown in Figure 1.5a. In the presence of 0.3 mM lactate, an evident peak arose at 0.52 V, which was resulted from the redox reaction of H_2O_2.[35] Figure 1.5b is the calibration curve of this enzyme electrode. The signal provided by the enzyme electrode, which was the current

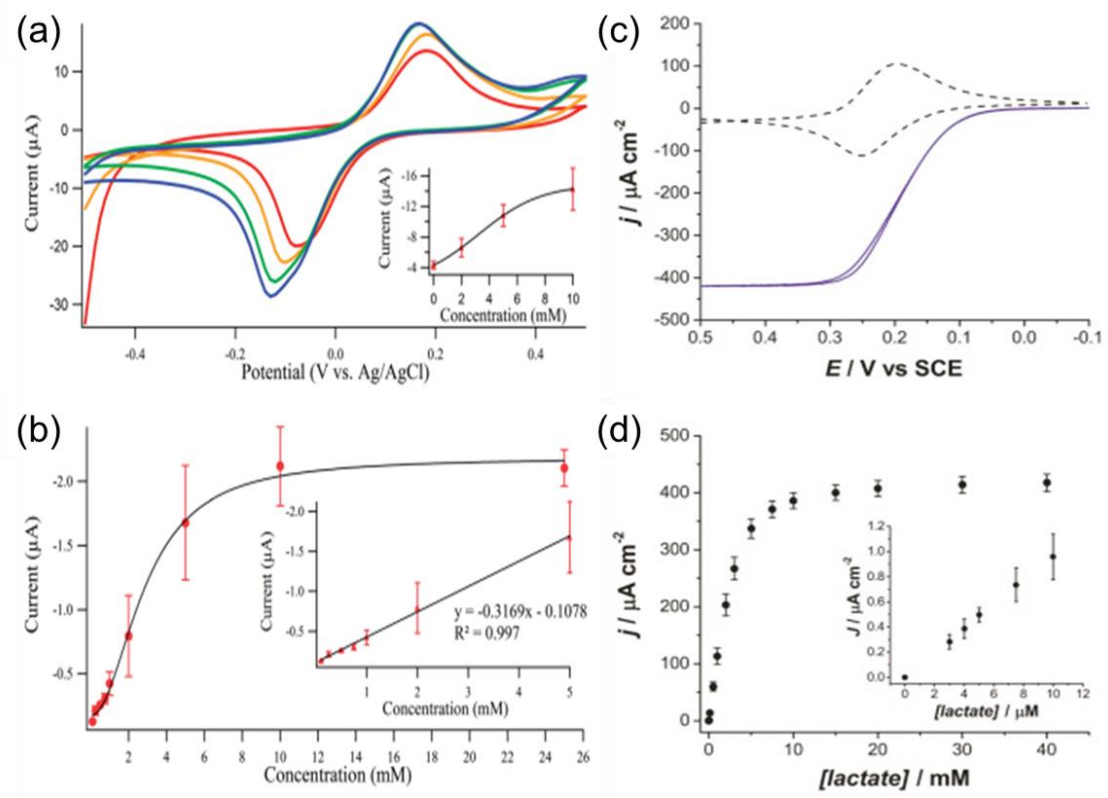

Figure 1.6. (a) The CV grams of the FED in various concentrations of lactate and (b) its response curve with an inset showing its linear detection range.[43] (c) The CV grams of the $FcMe_2$-LPEI/LOx film on a glassy carbon electrode in the PBS with (solid) and without (dashed) lactate. (d) The calibration curve of this enzyme electrode (Inset: the lower concentration range).[42]

density, increased linearly with the lactate concentration in the range of 3.6 μM to 0.6 mM and plateaued after 1.2 mM.[35]

The cyclic voltammograms (CV grams) in Figure 1.6a & c were generated by the lactate sensors in which redox mediators were incorporated. Comparing to the set of CV grams in Figure 1.5a, these two sets of CV grams differ greatly: they are the characteristic CV grams of reversible electrochemical reactions and there are background signals when no lactate is present.

Figure 1.6a was generated by a fabric-based electrochemical device (FED).[43] The WE surface of this FED was modified with Prussian blue (PB) which could transport electrons from the WE to H_2O_2. The signal detected by the FED was generated by the redox reaction of PB which was spontaneous and reversible on the WE surface. When the concentration of H_2O_2 increased, more electrons were transported by PB to reduce H_2O_2, resulting into a larger current.[43] As shown by the calibration curve of the FED, it had a linear detection range from 0.1 to 5 mM of lactate and its signal saturated at about 10 mM.[43]

The CV grams of a glassy carbon electrode coated with a film in 0 and 40 mM lactate solutions are presented in Figure 1.6c.[42] The film was composed of dimethylferrocene-modified linear polyethyleneimine and LOD. This ferrocene-modified polymer could facilitate the shuttle of electrons between the active site of LOD and the WE surface.[42] When more lactate molecules were catalyzed by LOD, more electrons were shuttled and the current increased. According to the calibration curve in Figure 1.6d, the signal of this enzyme electrode was linear to lactate concentration from 3 μM to 5 mM and it became saturated after 15 mM.[42]

As described before, all calibration curves presented in Figure 1.5 and 1.6 possessed similar features: the curve rises evidently with increasing lactate concentration in the beginning while plateaued after a certain level. In fact, all biosensors based on LOD should have this type of calibration curve which can be attributed to enzyme kinetics.

Michaelis–Menten kinetics is the most commonly used model to describe the enzyme

kinetics. In this model, the conversion from the substrate (S) to the product (P) catalyzed by the enzyme (E) involved an intermediate stage where S and E forms a complex ES. This process can be expressed as follows:

$$E + S \underset{K_{off}}{\overset{K_{on}}{\rightleftarrows}} ES \xrightarrow{K_{cat}} E + P \qquad 1.5$$

Where K_{on} and K_{off} are the rates of the binding and unbinding of E and S; K_{cat} is the rate of catalysis.[44] Michaelis–Menten equation can be derived from this reaction scheme under some assumptions. It describes the formation rate of P as follows:

$$\upsilon = \frac{d[P]}{dt} = \frac{v_{max}+[S]}{[S]+K_M} \qquad 1.6$$

where K_M is equal to (K_{off}+ K_{cat}) / K_{on} and υ_{max} is the maximum formation rate of P.[44] K_M indicates the strength of the binding between the enzyme and the substrates. A lower K_M means a tighter binding between the enzyme and the substrate which also indicates a less effective enzymatic reaction. By plotting this equation, one could get Michaelis–Menten saturation curve that shows how the concentration of S affects the P formation rate of an enzyme-involved reaction (Figure 1.7).[45] It is evident that the shape of the calibration curves of the lactate biosensors is similar to this Michaelis–Menten saturation curve.

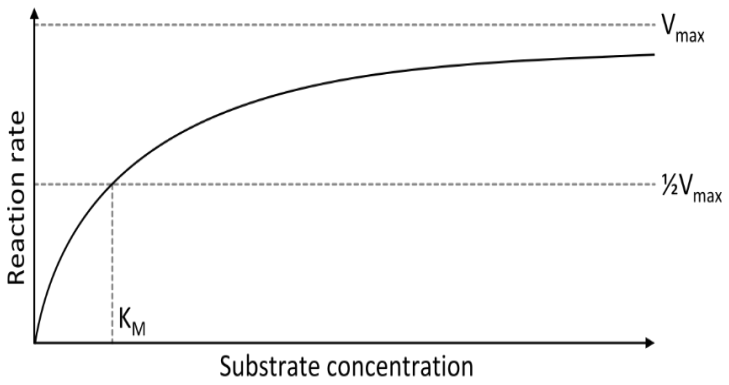

Figure 1.7. Michaelis–Menten saturation curve.[45]

Chapter 2. Electrode Fabrication and Modifications

2.1 Fabrication of Membrane Electrodes

2.1.1 Electron-beam Physical Vapor Deposition

Electron-beam physical vapor deposition (EB-PVD) is one technology that can coat a thin film of metal or ceramic on various types of substrates.[46] The membrane sensor in this work is made of thin-film gold electrodes that were fabricated using EB-PVD. The principle and advantages of EB-PVD will be briefly introduced.

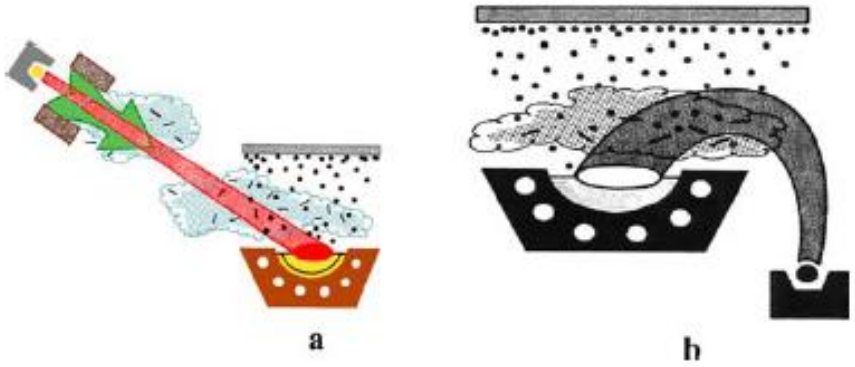

Figure 2.1. Two schematic representations of the EB-PVD process in which the electron beam is straight (a) and bent (b).[46]

The process of EB-PVD is presented in Figure 2.1. In a vacuum chamber, a strong and focused electron beam is directed straightly (Figure 2.1a) or bent (Figure 2.1b) to the material to be evaporated.[46] Taking the high energy from the electron beam, the material would melt, evaporate and deposit onto the substrate that is placed above it.[46] There could be extra electron beams in the chamber for preheating the substrate so that the coating on its surface would be more stable.[47,48]

Multiple types of materials can be placed in the chamber and be melt by the electron beam in sequence. Therefore, multilayer coating can be accomplished by EB-PVD without interrupting the vacuum.[47] Other significant advantages of EB-PVD can be listed as: having a higher deposition rate than other PVD techniques, controlled microstructure and composition, low contamination, and a smooth surface finish, etc.[47,49]

2.1.2 Fabrication of Thin-film Gold Electrodes

In enzymatic biosensors, the WE is normally made of highly conductive and electrochemically stable materials, such as gold, platinum and carbon.[50] Modifying these conventional electrodes with novel materials can improve their detecting performance.[50] For example, platinum nanoparticle ensemble-on-graphene hybrid nanosheet was decorated onto the surface of a glassy carbon electrode and successfully increased its sensitivity towards H_2O_2 detection.[51] Using gold nanoparticles and carbon nanotubes to modify electrode surfaces can help stabilize the enzyme molecules and facilitate electron transfer at the same time.[52,53]

At the beginning of this project, we wanted to keep all procedures simple. As a result, pure gold was chosen to be the material of all electrodes and no additional modification of the electrode material was included. The lactate biosensor was designed to be a three-electrode system. The electrodes were all made of pure gold on a vinyl sheet by EB-PVD. The structure of the three-electrode system was designed with the following important parameters: the diameter of the WE was 2.7 mm; the width of the RE and CE was 0.7 mm; the space between the adjacent electrodes was 1 mm; the straight tail of the electrodes was 23 mm long. The overall image of this three-electrode system is shown in Figure 2.2.

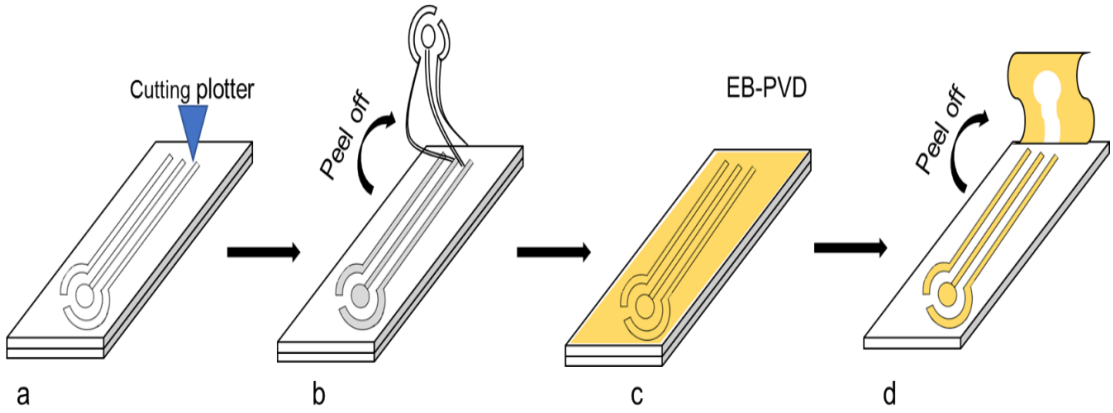

Figure 2.2. A schematic flow chart that shows the four steps in the electrode fabrication process.

Figure 2.2 shows the electrode fabrication process. First, one piece of vinyl sheet was adhered to another to form a double layer structure. This double layer vinyl sheet was then cut by a cutting plotter using a medium cutting strength so that the outlines of the electrodes are

formed only on the top layer (step a). In step b, those parts of the top layer inside the outlines were peeled off. Next, the double layer vinyl sheet with electrode patterns went through gold deposition by EB-PVD, during which 40 nm thick chrome and 200 nm thick gold were deposited in sequence (step c). The purpose of pre-depositing a layer of chrome is to enhance the adhesion between the substrate and the gold layer.[54] At last, the rest of the top layer was peeled off and the gold electrodes were successfully fabricated on the vinyl sheet (step d). Since the electrodes-on-vinyl construct were thin and flexible, they are referred to as membrane electrodes, hereafter.

Before further modification, the membrane electrodes were ultrasonic cleaned in isopropyl alcohol and liquid soap, each for 3 min, and rinsed by water. A 1 cm long optically clear adhesive membrane is attached to cover the straight stem portion of the electrodes as the insulating layer to define the active area of the electrodes. The active surface areas of CE, WE and RE are about 5.7, 5.7 and 2.4 mm^2, respectively. The counter electrode is made to have a relatively large surface area to ensure the stability of current.

2.2 Fabrication of Reference Electrode

2.2.1 Ag/AgCl Reference Electrode

The RE is an essential component in a biosensor that largely affects the accuracy and reliability of a sensor's response. There are several common reference electrodes, including Ag/AgCl electrode, calomel electrode and hydrogen electrode. Among these electrodes, the Ag/AgCl electrode is most widely used in research because of its simple structure and ease of manufacture.[39] The conventional macroscale Ag/AgCl electrode is typically a glass tube filled with a solution that has very high Cl^- concentration, in which a Ag wire with AgCl coating is immersed. The glass tube is enclosed by a porous membrane.[39]

The following reaction is the reaction inside the Ag/AgCl reference electrode:

$$AgCl_{(s)} + e^- \leftrightarrow Ag_{(s)} + Cl^-{}_{(aq)} \qquad 2.1$$

From this reaction, it is clear that the activity of chlorine ion has an effect on the electrode potential. Applying Nernst equation to this reaction, the potential of the Ag/AgCl

electrode could be expressed by the following equation:

$$E^{Cl^-|AgCl|Ag} = E^{0,Cl^-|AgCl|Ag} - \left(\frac{RT}{F}\right) lna_{Cl^-} \quad 2.2$$

where $E^{0,Cl^-|AgCl|Ag}$ is the standard potential of a Ag/AgCl electrode (0.23 V ± 10 mV against standard hydrogen electrode) , R is gas constant, T is temperature, F is Faraday constant and a_{Cl^-} is the ion activity of chloride ion in solution.[55] The ion activity is treated to be equal to the ion concentration under some specific conditions.

Ideally, the potential of one Ag/AgCl reference electrode should be constant. However, with the sustained use of the electrode, it might lose its ability to maintain the constant potential, resulting from the consumption of AgCl and the leakage of the internal filling solution.[39] To extend the lifetime of a Ag/AgCl electrode, it must be immersed in a Cl^- rich solution when it is not in use.

Conventional Ag/AgCl reference electrodes are bulk and have internal filling solutions, limiting their application in WHMDs. Therefore, solid-state reference electrodes (SSREs) were developed to replace conventional electrodes so that they can be assembled into miniaturized sensors.[56] Using SSREs also brings other benefits: the cost is greatly reduced; the mass production and maintenance of the electrode is simplified.[57] However, while conventional reference electrodes can maintain a constant potential for a long time, the potential of SSREs is not constantly stable in the test solution. The miniaturization of the Ag/AgCl electrodes greatly reduces the amount of Ag and AgCl in the electrodes, shortening their lifetime.[39] In some SSREs, Ag and AgCl were directly exposed to the test solution, leading to a greater variation of its potential.[58,59] To optimize the SSREs, the Ag/AgCl layer could be covered by a membrane with abundant Cl^- to play the role of a "solid filling solution".[39] For example, the agar gel saturated with Cl^- was used to modify the SSRE and successfully improve the stability of electrode.[60,61]

To fabricate the lactate biosensor of this project, which is supposed to be small-sized and flat, it is necessary to substitute the commercial reference electrode by a SSRE. The procedure of fabricating the SSRE will be introduced in the next section.

2.2.2 Fabrication of the Solid-state Ag/AgCl Electrode

SSREs are commonly made by three methods: electrochemical deposition[62], screen-printing[63] and sputter coating[64]. In this work, the solid-state Ag/AgCl electrode of the membrane electrodes was fabricated in two steps: 1. Depositing silver on the gold electrode by electrochemical deposition; 2. Oxidizing silver into silver chloride in 6% bleach. This method is cost effective and requires no specific equipment other than the electrochemical workstation which will be used to record the responses of the lactate biosensors to lactate concentrations later.

The equipment that was used to perform the electrochemical deposition was the CHI-650A electrochemical workstation from CHI Instrument, Inc. The RE and CE were purchased from the same company. $AgNO_3$ powder and NH_4OH solution were purchased from Sigma Aldrich.

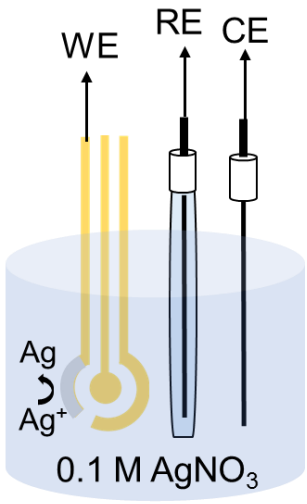

Figure 2.3. The setup for the electrochemical deposition of silver on gold electrode.

Figure 2.3 is a schematic representation of the setup for the electrochemical deposition of silver on one of the three membrane electrodes on a sensor. In this case, the RE of the membrane electrodes was used as the WE, a commercial Ag/AgCl electrode and a platinum wire were used as the RE and CE respectively. The electroplating solution was 3 mL of 0.1 M $AgNO_3$ in 1 M NH_4OH.

To begin the silver deposition, a constant potential of -0.1 V was applied for 30 s to

remove any microscopic gas bubbles on the electrode surface. Then, a constant potential of -0.5 V was applied for 20 min to deposit silver and during this process, the current change was recorded by the electrochemical workstation. After the silver deposition, the membrane electrodes were immersed in 6% bleach for 30 s so that part of the Ag was oxidized to AgCl. The active component of the bleach is NaOCl.

Taken out from the bleach, the electrodes were immersed in Milli-Q water and jiggled so that loosely bound AgCl could be washed away. In the end, all the membrane electrodes were gently wiped to dry.

During the whole process of the silver deposition, the WE and CE of the membrane electrodes stayed unchanged. When -0.1 V was applied, nothing varied on the surface of the RE of the membrane electrodes. As soon as -0.5 V was applied, a layer of ultra-thin silvery white coating appeared on the surface of the targeted electrode. Over time, this layer of silver grew thicker. Immediately after -0.5 V was applied, there was always a short period of time when the current decreased, which was due to the discharge of the electric double layer on the electrode.[65] The current variation recorded by the electrochemical workstation during the silver deposition was not exactly the same every time, but the current of a successful silver deposition should roughly increase from 0.8 to 3 mA after the short initial dip. On one hand, if the current was too small, there would be insufficient silver, leading to the instability of the solid-state Ag/AgCl electrode; On the other hand, if the current was too large, the deposited layer would become less uniform and there would be some silver aggregates which could easily fall off from the electrode surface. Under the normal deposition rate, the silver layer grew perpendicular to the electrode surface. However, the over-rapid growth of silver could lead to the lateral spread of silver to the surface of the adjacent electrodes. As a result, it was necessary to keep the current of silver deposition within the mentioned range.

Right after the electrode was placed in bleach, the silver layer turned black gray and little bubbles constantly arose from the Ag layer, indicating the formation of AgCl. Based on the production of gas in this process, the chemical mechanism of the silver reduction is

considered to be as follows:

$$2\mathrm{Ag}_{(s)} + 2\mathrm{NaOCl}_{(aq)} \rightarrow 2\mathrm{AgCl}_{(s)} + 2\mathrm{Na}_{(s)} + O_{2_{(g)}} \quad 2.3$$

2.2.2 Characterization of the Solid-state Ag/AgCl Electrode

To verify that the solid-state Ag/AgCl electrode functions properly as a RE, it was used to generate the CV grams of 0.5 mM $K_3Fe(CN)_6$ dissolved in 1 M KCl together with the WE and CE of the membrane electrodes. The CV grams were compared with the CV grams produced by using a commercial Ag/AgCl electrode. Three continuous CV scans were recorded using each (Figure 2.4).

The two sets of CV grams possess similar features in the shape. They both have two distinct peaks and the potential difference between the two peaks in one cycle is constantly 0.06 V. Based on this comparison, it is reasonable to say that this solid-state Ag/AgCl electrode is effective in terms of maintaining a constant potential for the WE.

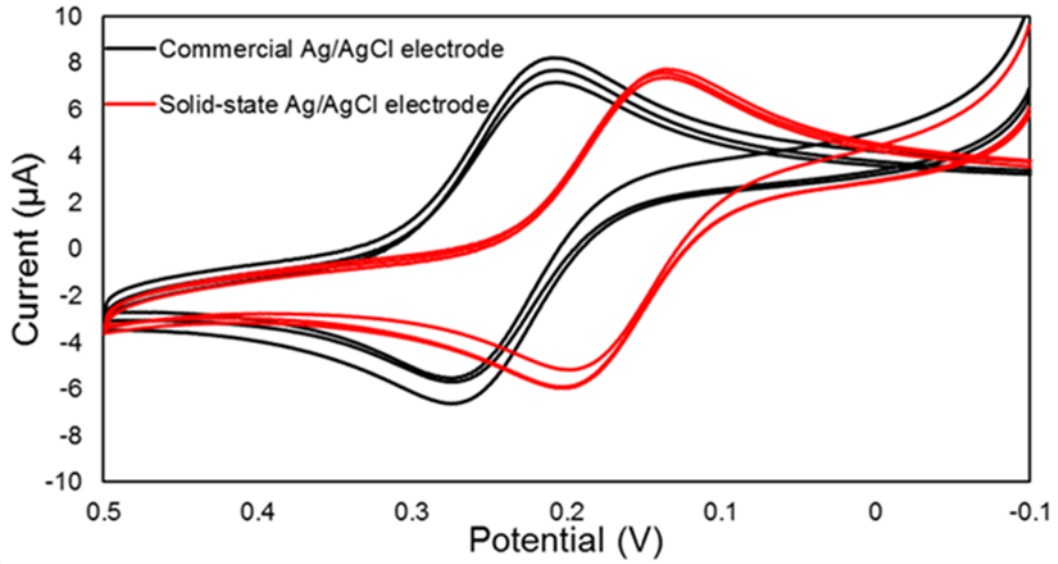

Figure 2.4. CV grams of 0.5 mM $K_3Fe(CN)_6$ in 1 M KCl. The potential of the working electrode is measured referring to a commercial Ag/AgCl electrode (black line) and the self-made solid-state Ag/AgCl electrode (red line).

However, there is a constant potential shift of about 0.07 V between the CV grams generated by the two different reference electrodes. The potential values shown in Figure 2.4 are the values of the actual potential applied on the WE subtracted by the offset potential of the reference electrode. Since the peaks of $K_3Fe(CN)_6$ have defined and positive potentials

versus absolute 0 V, and all Ag/AgCl electrodes have positive offset potentials, the reference electrode which leads to the smaller peak potential has the larger offset potential.

Based on Equation 2.2, the offset potential difference between two Ag/AgCl electrodes can be expressed as:

$$E_1 - E_2 = \left(\frac{RT}{F}\right) ln \frac{a_{Cl^-2}}{a_{Cl^-1}} \quad 2.4$$

If the electrode 1 is the solid-state Ag/AgCl electrode and the other is the commercial reference electrode, $E_1 - E_2$ will equal 0.07 V. According to Equation 2.4, the Cl^- activity of the commercial electrode turns out to be about 15 times larger than that of the solid-state Ag/AgCl electrode. That is to say, the Cl^- concentration in solution around the Ag/AgCl surface is much lower in the solid-state electrode than in the commercial electrode, which matches the reality. In the commercial electrode, the filling solution has 3 M Cl^-, while the solid-state electrode is immersed in the electrolyte solution that has 1 M Cl^-.

2.3 Modification of Working Electrode

2.3.1 Enzyme Immobilization Methods

The sensitivity and stability of the lactate biosensors strongly depend on the activity of LOD on the electrode surface. As a result, LOD immobilization is a key step in the fabrication of the lactate biosensor. There are two purposes of the enzyme immobilization: 1. Keeping the enzymes close to the electrode surface instead of diffusing into the test solution; 2. Providing a friendly environment to the enzymes so that they will not be denatured, and their active sites can function properly.

Many enzyme immobilization methods have been reported and they can be classified in five categories (Figure 2.5).[66] Depending on the type of interaction between enzymes and the electrode, they can be further identified as chemical or physical immobilization. Covalent and cross-linking are chemical immobilization methods. For covalent, enzymes form covalent bonds with the electrode whose surface is coated with polymers through carboxylic and amino groups. For cross-linking, enzymes are cross-linked by crosslinkers with each other or

with other inert proteins.[66]

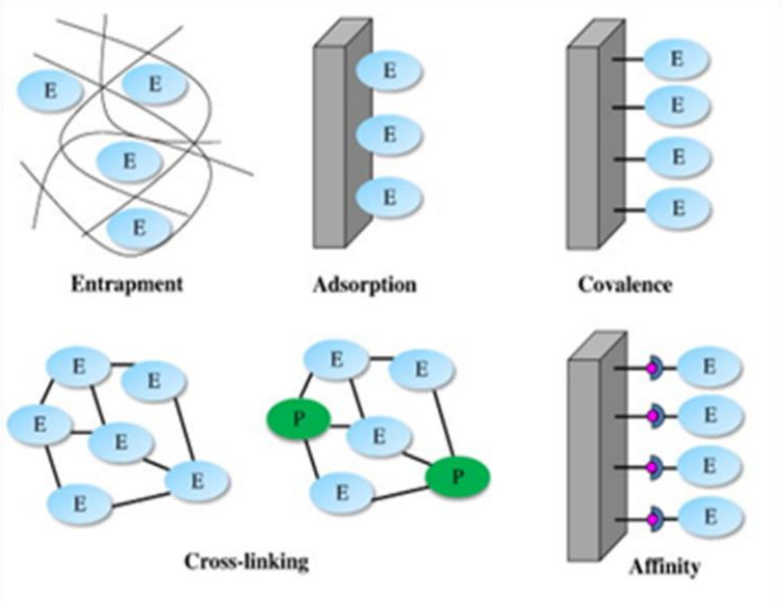

Figure 2.5. Schematic drawings of five enzyme immobilization methods.[66]

Other three methods are physical immobilizations. Enzyme entrapment means that enzymes are encapsulated into a three-dimensional gel or polymer network. Adsorption means that enzymes interact with the substrate through weak forces, such as van der Waal's forces and electrostatic interactions. Affinity relies on the affinity of enzymes towards a modified electrode resulted from some specific protein sequence, which is similar to the antibody-antigen interaction.[66]

Using chemical immobilization, enzymes are fixed in a stable way but can lose a lot of their activities. On the other hand, physical immobilization may have the problem of enzyme leaching but retains enzyme activity to the greatest extend.

Although most loss of enzyme activity is caused by their denaturation, the random orientation of enzymes on the electrode surface is another significant reason. Those enzymes whose active site are not exposed to the test solution might have difficulty interacting with their substrates.[66] Specifically designed covalent and affinity immobilization methods are able to immobilize enzymes in an ordered and oriented way, which further boost the general activity of enzymes.[67,68]

Nanomaterials such as carbon nanotubes and a variety of nanoparticles are popular

materials to immobilize enzymes. As mentioned before, carbon nanotubes are highly conductive and facilitate the electron transfer between the enzymes and the electrode; meanwhile, they can provide mechanical and structural support to the enzymes.[69] Nanoparticles have high conductivity as well. They provide a larger surface area for enzymes than the macro electrode surface dose, reducing the denaturation of enzymes.[67,70]

2.3.2 Immobilization of LOD

In this work, LOD was immobilized together with bovine serum album (BSA) cross-linked with glutaraldehyde (GA). GA is considered as the most widely used and the most effective cross-linker of proteins.[71] It can react with several functional groups of amino acids.[72] In enzyme immobilization, GA primarily forms covalent links with the lysine groups of enzymes.[73,74] As a result, when inert and lysine-rich proteins, such as BSA, are co-immobilized with enzymes, the process of cross-linking becomes more effective.[75] It is proven by previous work that when enzymes are co-immobilized with BSA, the loss of their activity could be reduced, and the response of biosensors could be more accurate.[75–77]

Figure 2.6A clearly shows the binding between GA and the enzyme, in which the AL

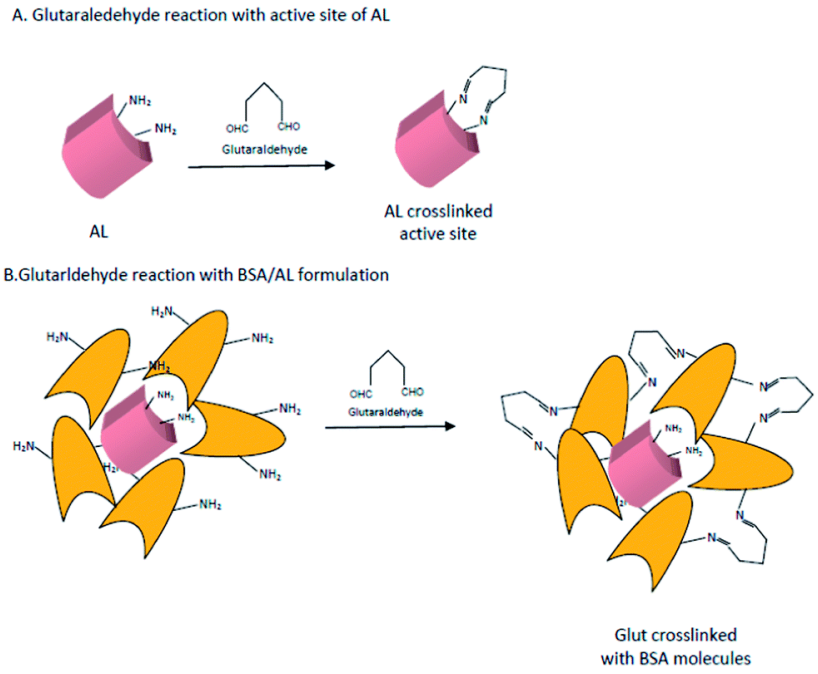

Figure 2.6. Schematic presentations of the enzyme crosslinking using GA in the (A) absence and (B) present of BSA.[78]

stands for alginate lyase and could represent all enzymes.[78] GA forms C=N bonds with the ϵ-amino groups of the enzymes.[72,78] If these ϵ-amino groups exist at the active site, this enzyme is deactivated. When a large amount of BSA is present in this matrix, GA molecules are more likely to react with BSA as presented in Figure 2.6B.[78] Therefore, modifications to the active sites of the enzymes will be reduced.

To immobilize LOD on the WE of the membrane electrodes, LOD lyophilized powder was purchased from AG Scientific. 25% GA solution and BSA lyophilized powder were purchased from Sigma Aldrich. 10× PBS was purchased from EMD.

10× PBS was diluted to 1× PBS with Milli-Q water. 20 mg/mL LOD solution and 150 mg/mL BSA solution were prepared by dissolving their powder in 1× PBS. 25% GA solution was diluted to 10% using Milli-Q water. Both the LOD and BSA solution was light yellow and the GA solution was transparent.

The enzyme immobilizing matrix was composed of 7.5 μL BSA, 7.5 μL GA and 10 μL LOD solutions. The matrix was freshly prepared by mixing the three solutions every time before use. During the mixing of the solutions, bubbles occurred easily and were hard to remove. As a result, after mixing, only 13 μL of the mixture, in which no bubbles exist, was dropped onto the surface of the WE. The electrode was then left in the fume hood and exposed to the air for 40 min. Afterwards, the liquid mixture turned from a hemisphere into a flatter and gel-like membrane that covered the whole WE. The color of the mixture also turned light brown from light yellow.

After the enzyme immobilization, the electrodes were immediately used for the following tests instead of being stored by any means. Before being used, the electrodes were washed by a gentle flow of Milli-Q water to get rid of the unbound substance and dabbed to dry.

After the preparation of the solid-state Ag/AgCl electrode and the enzyme electrode, the membrane sensors were ready to be used for lactate detection in liquid samples.

Chapter 3. Electrochemical Detection of Lactate

3.1 Cyclic Voltammetry and Differential Pulsed Voltammetry

Two electrochemical techniques, CV and differential pulse voltammetry (DPV), were used for recording the electrochemical responses of the membrane sensors in this work. These two techniques were performed by the CHI-650A electrochemical workstation (CHI Instrument, Inc.). The principle of CV and DPV are introduced in this section.

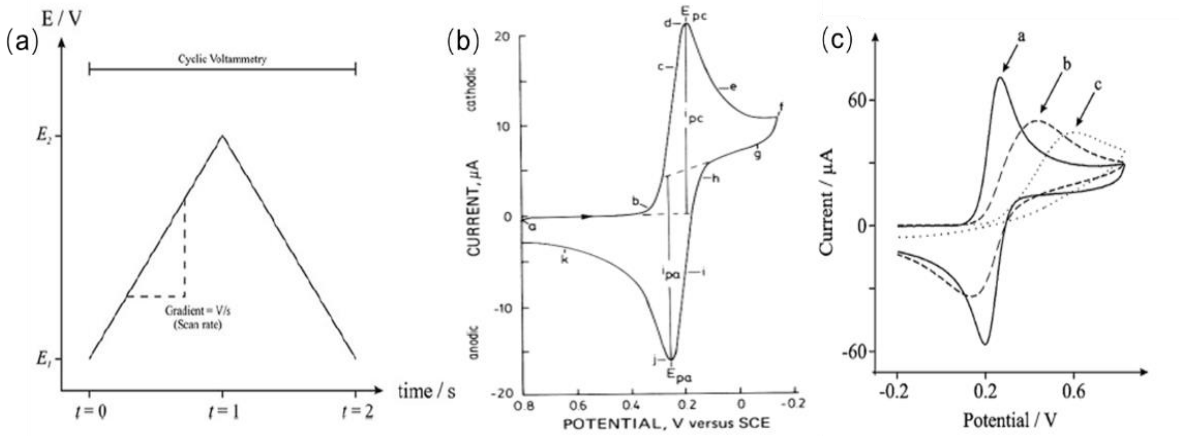

Figure 3.1. (a) The potential-time profile of one cycle in CV.[79] (b) The cyclic voltammogram of 6 mM $K_3Fe(CN)_6$ in 1 M KNO_3 (SCE: saturated calomel electrode, scan rate: 50 mV/s).[80] (c) Examples of CV grams of a. reversible, b. quasi-reversible and c. irreversible electrochemical reactions.[79]

CV is a measurement of the current value at the WE when the potential applied on it cycles between two set values with a certain scan rate as shown in Figure 3.1a.[79] CV gives an insight into redox reactions. Figure 3.1b is an example of CV gram which is the CV gram of 6 mM $K_3Fe(CN)_6$ in 0.1 M KNO_3 solution.[80] During the forward scan, from 0.8 V to -0.2 V, when the potential becomes negative enough, $Fe(CN)_6^{3-}$ gets reduced into $Fe(CN)_6^{4-}$ and results into a cathodic current. In the reverse scan, from -0.2 V to 0.8 V, when the potential is positive enough, $Fe(CN)_6^{4-}$ gets oxidized back to $Fe(CN)_6^{3-}$ and an anodic current is formed.[80] Such an electrochemical reaction is defined to be reversible and produces the most typical CV gram with two defined peaks. Meanwhile, other electrochemical reactions could be quasi-reversible and irreversible, generating CV grams like plot b and c in Figure 3.1c,

respectively.[79] In the CV gram of an irreversible reaction, only one peak could be observed.[79]

There are established equations that express the magnitude of I_p for the different types of CV grams. For example, when a macroelectrode is used, the I_p of a reversible and irreversible CV could be defined by Equation 3.1 and 3.2:

$$\text{Reversible: } I_p^{Rev} = \pm 0.446nFAC(nFD\upsilon/RT)^{1/2} \quad 3.1$$

$$\text{Irreversible: } I_p^{Irrev} = \pm 0.496(\alpha n')^{1/2}nFAC(FD\upsilon/RT)^{1/2} \quad 3.2$$

where F and R are Faraday's constant and the gas constant, respectively; υ is the scan rate; T is the temperature; A is the area of the electrode surface; n and n' are the numbers of electrons transferred per mole during the whole process and before the rate determining step, respectively; α is the transfer coefficient; D is the diffusion constant of the reactant; C is the concentration of the reactant.[79] As a result, by keeping all the other parameters the same, one could get a I_p from CV that is solely determined by the concentration of the reactant.

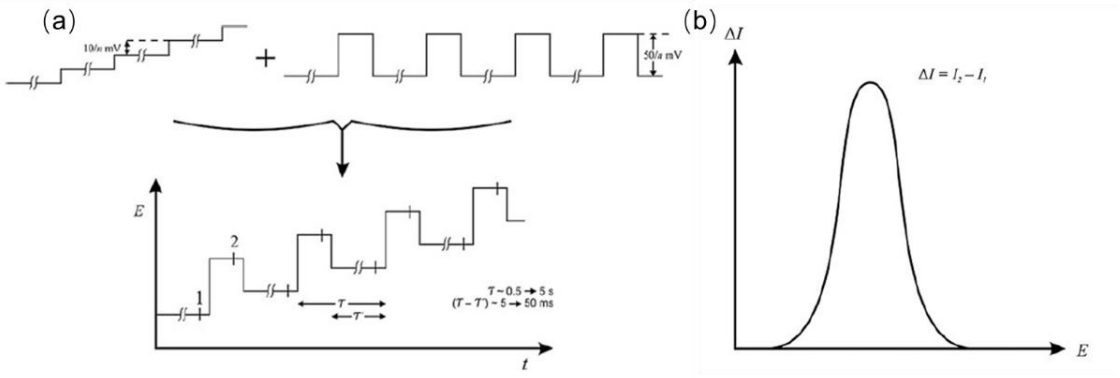

Figure 3.2. (a) The potential-time profile of DPV. (b) A typical DPV gram.[79]

Different from CV, DPV has a potential profile which is a combination of staircase and pulse as shown in Figure 3.2a.[79] By applying potential in this way, the capacitative current caused by the double-layer charging at the electrode surface could be eliminated. As a result, the current detected by DPV is pure Faradic current. Figure 3.2b is a typical DPV gram.[79] The current presented in a DPV gram is the difference between two values, I_2 and I_1, which is recorded at the point 2 and 1 as labelled in Figure 10a, respectively. DPV is normally used instead of CV to enhance signal or distinguish two close peaks. The same as CV, the I_p

of DPV is proportional to the concentration of the reactant when all the other conditions remain unchanged.[79]

3.2 Cyclic Voltammogram of Lactate

To get an overall understanding of the electrochemical behavior of lactate, the CV gram of lactate was firstly generated by a standard three-electrode system within a large potential range (between 0.65 V and -0.5 V). The standard three-electrode system was composed of commercial electrodes: a 2 mm-diameter gold disk electrode as the WE, a platinum wire as the CE and a commercial Ag/AgCl electrode as the RE. LOD was immobilized on the WE by the same enzyme immobilization method introduced in Section 2.3.2 while 15 µL of the mixture was dropped onto the WE surface. All electrodes were fixed by a Teflon cap so that the distances between three electrodes and the active surface area of the CE were consistently the same.

Before the electrodes were used to detect lactate, they were activated by several CV scans in 1× PBS. Seven beakers were prepared, each containing 4 mL 1× PBS with various concentrations of lactate as listed in Figure 3.3. The electrodes were placed into one beaker and one cycle of CV was performed. Before every CV scan, there was a 10 s quiet time.

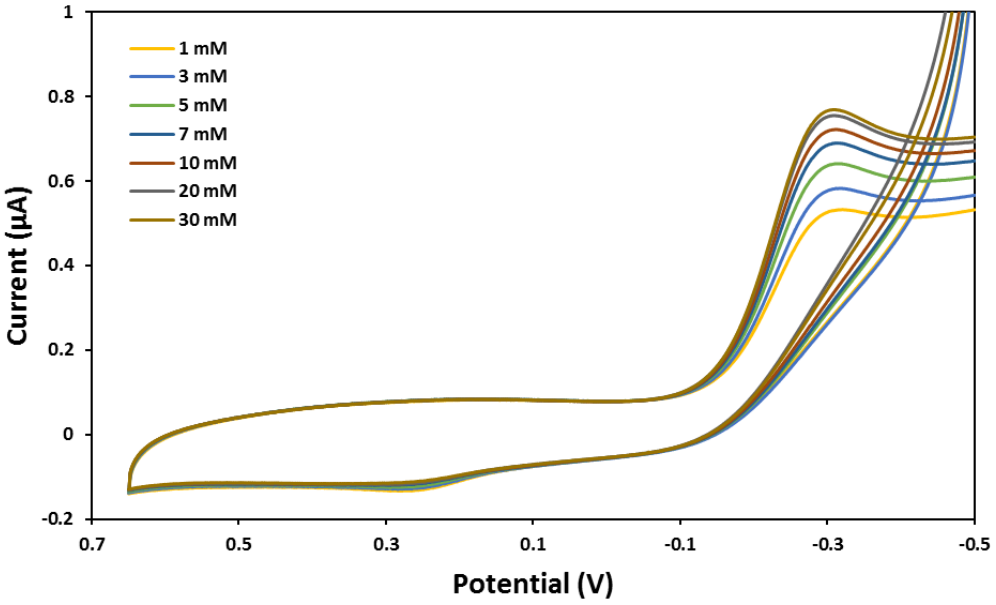

Figure 3.3. The standard CV grams of different concentrations of lactate in PBS. (Scan rate: 0.01 V/s)

When the test in one beaker was completed, the electrodes were taken out, rinsed by Milli-Q water, dabbed to dry and immediately placed into the next beaker for the next CV scan. The lactate solutions were detected by the electrodes from the lower to higher concentration.

The standard CV grams of different lactate concentrations that were generated by the standard electrode system are shown in Figure 3.3. In each CV gram, there are two peaks. During the positive scan, from -0.5 V to 0.65 V, there is a small peak between 0.2 and 0.4 V, but it declines as the lactate concentration increases. It is not clear that where this peak originates from. During the reverse scan, from 0.65 V to -0.5 V, there is an evident and defined peak at -0.3 V. This peak grows when the lactate concentration in the solution increases. According to the definition of the peaks in CV grams introduced in Section 3.1, the second peak is recognized as the cathodic peak that represents the reduction of H_2O_2.

There should be an oxidation peak of H_2O_2, however, it is not observed in all the CV grams. Since the lactate biosensor is required to work within a low potential range (whether negative and positive) and it turned out that the reduction peak appeared at a lower potential than the oxidation peak, no attempt was made to find the oxidation peak.

Based on this set of standard CV spectra of lactate, the potential range of interest of the following electrochemical tests was determined to be smaller than 0 V so that the reduction peak of H_2O_2 would be detected to represent the concentration of lactate.

3.3 Lactate Detection by the Membrane Sensors

After the successful detection of lactate in PBS by the standard electrode system, the responses of the membrane sensors to lactate were tested by CV using a similar procedure. As introduced in Chapter 2, the membrane sensors had a LOD-immobilized WE, a gold CE and a solid-state Ag/AgCl electrode.

In total, three membrane sensors were tested. All membrane sensors were activated in 1× PBS by several CV scans. In each test, there were seven beakers that each contained 4 mL 1× PBS with the lactate concentration of 1, 3, 5, 7, 10, 20 and 30 mM. One membrane sensor was placed into the beakers in sequence, from the lower to higher lactate concentration, and

one CV gram was recorded in each beaker. Before every CV scan, there was a 10 s quiet time. Every time that the membrane sensor was taken out from one beaker, it was rinsed by Milli-Q water and dabbed to dry.

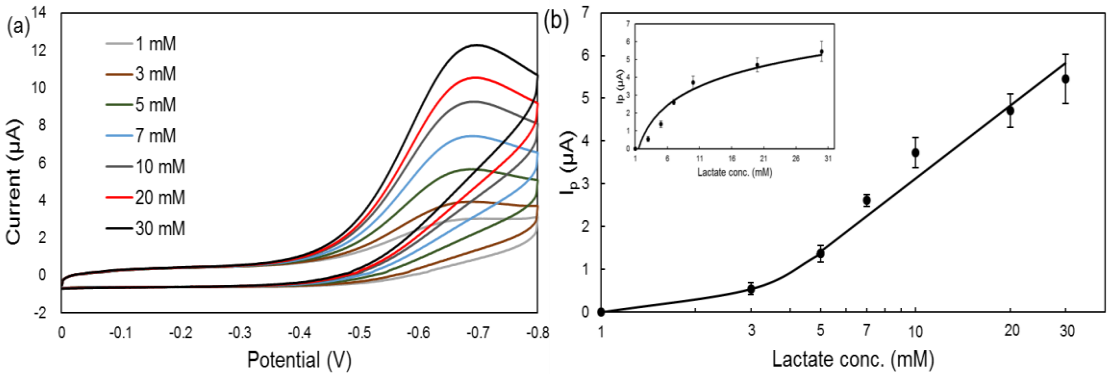

Figure 3.4. (a) The CV grams of a membrane sensor in 4 mL PBS with different lactate concentrations (1-30 mM). (scan rate: 0.05 V/s) (b) The calibration curve of the membrane sensors in PBS which shows the change of I_p over lactate concentration on a semi-logarithmic scale. Inset: the original calibration curve.

Figure 3.4a is a set of the CV grams produced by one of the membrane sensors. The potential range is between 0 and -0.8 V. The scan rate is 0.05 V/s, which is five times of the scan rate of the CV in section 3.2. The reason why the potential scan was accelerated was that under a very slow scan rate, like 0.01 V/s, the membrane sensor produced unstable signal instead of a smooth curve, which might have resulted from the solid-state Ag/AgCl electrode. This generated reference electrode might not be able to control the potential as precisely as the commercial reference electrode can do.

In every CV gram in Figure 3.4a, there is an evident peak. Different from the position of the H_2O_2 peak generated by the standard electrode system, the H_2O_2 peak in Figure 3.4a is located around -0.65. The huge shift of H_2O_2 peak from -0.3 V (in Figure 3.3) to -0.65 V can be partly explained by the replacement of the commercial Ag/AgCl electrode by the solid-state Ag/AgCl electrode. The Cl^- concentration of 1× PBS is 0.14 M, which is much smaller than that of the filling solution (3 M) in the commercial Ag/AgCl electrode. If we consider the activity of Cl^- the same as its concentration and the $\frac{a_{Cl^-2}}{a_{Cl^-1}}$ in equation 2.5 equals to 3 M divided by 0.14 M which is 21.4, we will get the potential difference between two reference

electrodes as 0.078 V, which is much smaller than the actual potential shift. The use of a gold CE, instead of a platinum wire, could also contribute to the shift of peak position.

The absolute values of I_p generated by different membrane sensors in the same lactate concentration varied from one sensor to another. However, after baseline correction, i.e., subtracting the I_p of 1 mM from each I_p, the calibration curves of three membrane sensors could be presented in one plot. The inset of Figure 3.4b is the original calibration curve of the membrane sensors. It can be seen that I_p increases almost linearly with the lactate concentration in the range of 1 to 10 mM. However, after 10 mM, the slope of the change of I_p becomes smaller, which means the signal starts to saturate, as expected.

From every membrane sensor, K_M and V_{max}, which are the essential parameters in Michaelis–Menten equation, can be calculated out to characterize the LOD immobilization on the electrode. The mean values of these two parameters is K_M = 8.18 (± 2.30) mM and V_{max} = 6.55 (± 1.17) μA. There are large deviations among the three membrane sensors, indicating that each enzyme electrode varies from each other. As stated before, after LOD, BSA and GA are mixed, only 13 μL of the mixture is used. If LOD is not uniformly distributed, the total amount of LOD on the WE will be inconsistent for the sensors. After being crosslinked, the amount of LOD whose active site has been modified varies every time, altering the amount of active LOD. A larger amount of active LOD is likely to result into a larger current. The immobilization not only chemically modifies LOD but also fixes its orientation. Therefore, the affinity between lactate and LOD, represented by K_M, is different in each enzyme matrix. During the 40-min crosslinking process, the enzyme matrix is also dried by air flow. Its thickness can be affected by its surface area as well as the flow rate and humidity of the air. Since the total amount of BSA and LOD varies, the density of these two is even more inconsistent in the enzyme matrixes considering their varying thickness. The protein density influences the mass transport of lactate and H_2O_2 inside the enzyme matrix, thus likely to bring changes to both K_M and V_{max}.

Since we are interested in the abnormal high lactate level in the human body, a larger

dynamic response range is desirable. The calibration curve in Figure 3.4b is established on the logarithmic values of lactate concentrations. In this way, the dynamic range of our membrane sensors is 4 to 30 mM. The detection limit (30 mM) is larger than the highest physiological lactate level stated in Section 1.3 (18 mM).

Two essential parameters, limit of detection (LoD) and sensitivity, can be derived from the calibration curves. LoD is the minimal detectable concentration and is defined as $3.3*\sigma_1/s_1$, in which σ_1 and s_1 are the standard deviation of response and the slope of the original calibration curve, respectively.[81] Based on the linear range of the original calibration curve, the LoD of the membrane sensors is calculated to be 1.54 mM. Sensitivity (ΔC_{min}) is defined as the minimal difference between two distinguishable concentrations C_1 and C_2 ($C_1<C_2$). It is calculated following this equation: $\Delta C_{min} = C_2–C_1 = (C_2/C_1–1)*C_1 = \{10\text{^}(3.3*\sigma_2/s_2)–1\}*C_1$. σ_2 and s_2 are the standard deviation of response and the slope of the semi-log calibration curve, respectively. The ΔC_{min} of the membrane sensors is determined to be $0.78C_1$ mM in the linear range of the semi-log calibration curve. That is to say, for the membrane sensors, the sensitivity is lower at higher analyte concentration.

Chapter 4. Transdermal Detection of Lactate

4.1 Distribution of Body Fluid in Skin

Most biosensors require liquid samples. For biosensors in WHMDs, various body fluids can be collected as samples to monitor various health indicators, including interstitial fluid (ISF), sweat, tear and saliva.[82–85] In terms of lactate detection, it was reported that capillary blood lactate levels correlate well with systemic blood lactate levels in both steady and varying states.[86] In ISF, the lactate level is higher than that in blood at rest and it follows the blood level with a 30-min delay.[87] As a result, to monitor lactate level in the human body, ISF and capillary blood are reliable substitutes of systemic blood.

The distribution of ISF and capillary blood in the human skin is shown in Figure 4.1. Skin is the largest organ of human body.[88] The epidermis is the outermost layer of skin with a thickness varying from 50 to 150 μm. It is a protective layer of the human body without blood vessels.[89] Beneath the epidermis is the dermis which has a large amount of ISF.[90] ISF constitutes about 45% of skin volume and contains many analytes of interest since it transports materials and molecules between cells and blood capillaries, cells and cells.[89] At a

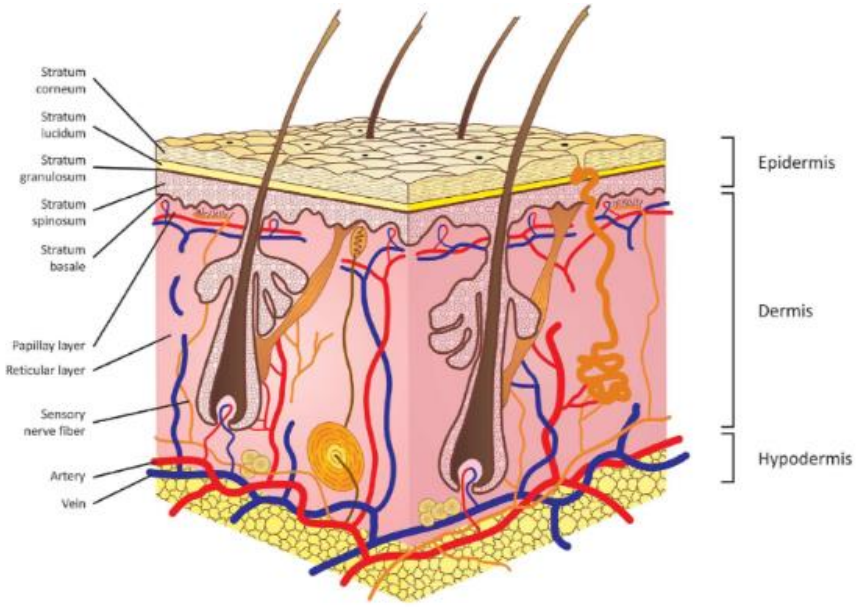

Figure 4.1. A schematic representation that shows the structure of the three layers in the human skin, including the epidermis, dermis and hypodermis.[89]

depth of 300 to 600 μm from the skin surface, there is a superficial plexus, composed of small capillary blood vessels.[89] Capillary blood is a good substitute for systemic blood in terms of health inspection. It originates from systemic blood, having the same constituents at similar concentrations.[89]

4.2 Extraction of ISF and Capillary Blood

The transdermal extraction of ISF and capillary blood is minimally invasive to human body compared to the collection of systemic blood, making WHMDs more suitable for daily use. For a WHMD, although a high-quality sensor is essential, the way of collecting body fluids can also strongly influence its acceptability to the users. There are some extraction methods that can be used at home by untrained people. The most direct method is using a lancet to pierce skin. Several more comfortable ways involve the use of laser ablation, ultra sound and reverse iontophoresis.[91] Laser ablation and ultra sound can open pores in the epidermis so that some ISF is released. Reverse iontophoresis works by building up an ion flow across the skin so that analytes can be extracted out of the skin with this ion flow.[91]

With the development of fabrication technology on the micrometer level, various types of microneedle arrays have been produced and used in transdermal applications, including drug delivery and body fluid extraction. Since Henry *et al.* first applied silicon microneedles to deliver a model drug through the epidermis in 1998, microneedle arrays have experienced extensive usage in transdermal drug delivery.[93,94] In this field, both solid and hollow

	Hollow microneedle array	
Function	Extract capillary blood	Extract interstitial fluid
Penetration depth	400–900 μm	50–150 μm
Lumen diameter	At least 50 μm	At least 10 μm
Material	Higher strength	Relatively lower strength

Table 4.1. Requirements for hollow microneedles which are used to extract body fluids.[92]

microneedle can be used.[93] While to extract body fluid out of the human body, hollow microneedles are required. Some basic requirements for hollow microneedles are listed in Table 1.

As mentioned previously, Henry *et al.*'s microneedle arrays were made of silicon.[86] Silicon has been verified to have short-term biocompatibility.[95] However, the long-term influence of silicon to the human body is not clearly defined. Meanwhile, silicon is brittle and expensive, which further prompted scientists to find other materials to make microneedles.[96] For example, there have been microneedles made of polymers and sugars[97–100]. Such materials are better than silicon in terms of their degradability in the human body.[96]

Although microneedles can have various dimensions all of them are expected to be minimally invasive to the human body and cause very slight pain. This was determined by one research where microneedle arrays with 5 or 50 microneedles that have different lengths (480 to 1450 μm), widths (160 to 465 μm) and thicknesses (30 to 100 μm) were applied on the volar forearms of ten healthy human subjects. Comparing to a hypodermic needle, these microneedle arrays caused 60 to 95% less pain to the subjects.[101]

In conclusion, transdermal extraction of body fluids can be accomplished by microneedles. In this project, two kinds of transdermal microneedle patches that were manufactured by 3M Canada were used. These transdermal patches were originally made for transdermal drug delivery so that their biocompatibility was guaranteed. Referred to as long needles and short needles, they are 1500 and 1000 μm long, respectively. Each microneedle patch has 12 microneedles lined in a circular shape and the lumen diameter of all microneedles is 80 μm. All microneedle patches are made of liquid-crystal polymer.

4.3 On-skin Operation of the Membrane Sensor

The ultimate goal of this project is to fabricate a device that can quantify lactate level transdermally. That is to say, this device should be able to collect and detect the body fluid simultaneously. For this purpose, we attached the lactate membrane sensor as described in Chapter 3 to the transdermal microneedle patch from 3M Canada.

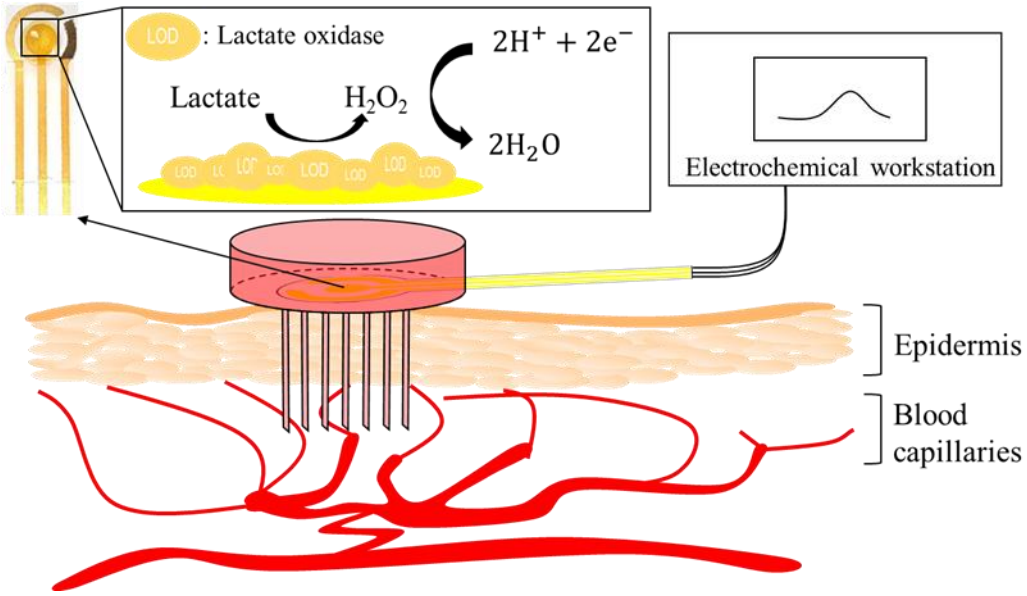

Figure 4.2. A schematic representation of the transdermal lactate sensor.

Figure 4.2 is an illustration of the general concept of lactate detection conducted using our device. As introduced before, to collect capillary blood, the penetration depth of the microneedles should be 400 to 900 μm.[92] Our microneedles are 1500 and 1000 μm long so that they are expected to be able to reach the blood capillaries when they are inserted into the human skin. As a result, the body fluid sample that is extracted out is likely to be a mixture of capillary blood and ISF. On top of the transdermal patch, there is a chamber to accommodate a small volume of the extracted body fluid. A membrane sensor is attached to the transdermal patch and situated inside this chamber. When enough body fluid is collected (>100 μL), the sensing electrodes will be immersed in the fluid and the enzymes on the WE will start to oxidize lactate. The tail of the membrane sensor extends out of the chamber so that it can be electrically wired to the electrochemical workstation. As soon as a proper potential is applied to the WE, H_2O_2 will be reduced and current will be produced. The current will be detected and recorded by the electrochemical workstation. This electrical signal will be sent to and analyzed by another device. This device will translate the electrical signal into the lactate concentration based on the calibration curve of the membrane sensor.

For proof of concept, a sensor-enclosing device (SED) was fabricated, using which

sample collection and detection of lactate were demonstrated. The procedure of fabricating the SED is described in the next section.

4.4 Fabrication of the Sensor-enclosing Device

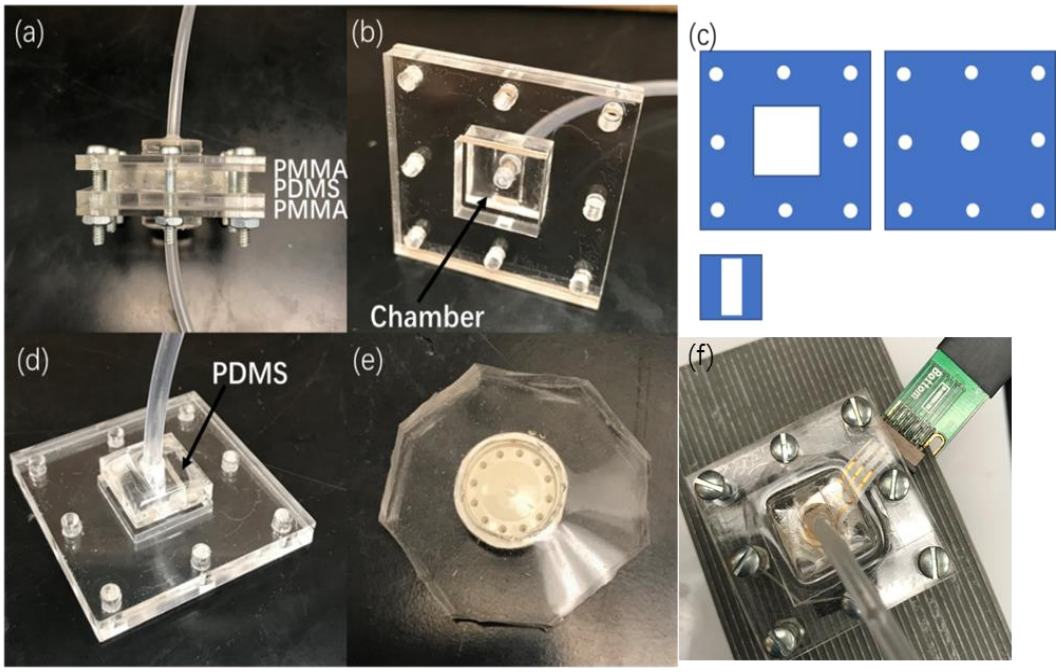

Figure 4.3. A picture of (a) the SED and (b) the PMMA layer. (c) A schematic drawing of three PMMA pieces that constitute the PMMA casing. A picture of (d) the tube fixation by PDMS and (e) the PDMS layer holding the transdermal patch. (f) A picture of the membrane sensor assembled inside the SED and connected to the external circuit.

Poly(methyl methacrylate) (PMMA) and Polydimethylsiloxane (PDMS) are the main materials that constitute the SED. PMMA plates are cut into desired shapes using a laser cutter. PDMS is made by mixing the base and curing agent with a weight ratio of 10:1 and curing the mixture at 80 °C overnight.

Figure 4.3a is a picture of the whole SED. This device can be disassembled into three layers. The upper and bottom layers are made of PMMA. The middle layer is made of PDMS. Figure 4.3b shows the chamber and the small tube connecting to the chamber through the PMMA casing. Each PMMA casing consists of three pieces of PMMA bonded together (Figure 4.3c). The first and second pieces of PMMA have a big square hole and a small circular hole in the middle, respectively. After being glued together, these two pieces of PMMA form the chamber. The last piece of PMMA is made for the tube fixation. After the

tube is inserted into the middle hole, liquid PDMS is poured into the gap between the tube and the small PMMA piece (Figure 4.3d). When the PDMS gets solidified, liquid leakage between the tube and the PMMA is prevented.

Figure 4.3e displays the middle PDMS layer holding a transdermal patch. The hole of the PDMS layer is made to be smaller than the transdermal patch so that when the transdermal patch is placed into the PDMS layer, it is held very tight. There is no gap between the transdermal patch and the PDMS so that the only path for liquid to transfer between the top and bottom is through the microneedles. The membrane sensor is glued onto the back of the transdermal patch by epoxy. When the membrane sensor is placed in the device, it can be connected to the external circuit as shown in Figure 4.3f.

When the membrane sensor and the transdermal patch are pressed onto the human skin, body fluid will be extracted out through the microneedles and immerse the sensor. This process can be mimicked by pumping liquid into the SED using a syringe through the bottom tube.

4.5 Mass Transport through the Microneedles

The microneedles have an extremely small radius which means they have the potential to suck liquid up by capillary force. However, these microneedles have hydrophobic surface that will hinder the flow of liquid. As a result, when a transdermal patch pierces the human skin, body fluids is not likely to be automatically extracted out. To facilitate the extraction, a vacuum or low-pressure environment is probably required outside the skin to create a pressure difference across the transdermal patch.

To provide some hints about how much the pressure difference across the transdermal patch should be to reach a desired flow rate of liquid extraction, a mass transport experiment was performed.

4.5.1 Materials and Methods

In each mass transport experiment, one transdermal patch was placed inside the SED with its needle tips facing down. The experimental setup is shown in Figure 4.4a. The bottom

tube of the device is connected to a burette. The burette contains a certain amount of liquid and is used to create the pressure that leads to the liquid transport from bottom to up through the microneedles in the device. The specific value of the pressure is calculated according to the equation below:

$$\Delta P = \rho g h \quad (4.1)$$

where ρ is the density of the liquid used, g is the gravitational constant and h is the height difference between the liquid surface in the burette and the end of the upper tube.

Two types of liquid were tested, water and a glycerol solution. The glycerol solution was a mixture of 55 % water and 45 % glycerol (by weight). This mixture had a dynamic viscosity of 4.4 cP at room temperature which is similar to the dynamic viscosity of human whole blood at 37 ºC.[102] Before each experiment, the liquid was filled up to the end of the upper tube of the device. Each mass transport experiment lasted for 3 min during which the valve of the burette was kept open and extra water or glycerol solution was constantly added into the burette to maintain a constant liquid level. After 3 min, the mass of the liquid extruded from the upper tube, collected in the small beaker, was weighed and converted into its volume. For calculation, the water density was treated as 1 g/cm^3 and the density of the glycerol solution was 1.1126 g/cm^3. The average flow rate of the mass transport was calculated by dividing the volume of transported liquid by 180s.

4.5.2 Results and Discussion

The results of the mass transport experiment are presented in Figure 4.4b. As indicated by the small error bars in Figure 4.4b, by maintaining a constant height of liquid in the burette, a cross-patch pressure (up to 3000 Pa) can be stabilized at a certain value very accurately during the 3-min test. The transport rates of water and glycerol solution increases linearly with increasing pressure. This linear relation also indicates that the SED is sealed well: there is no air or liquid leakage. Comparing among four tests, the flow rate profiles possess four different slopes. Under the same pressure, both water and glycerol solution have a higher flow rate when they are transported through short needles. Water, the liquid with

lower viscosity, always has a higher transport rate than the glycerol solution when the driving force is the same.

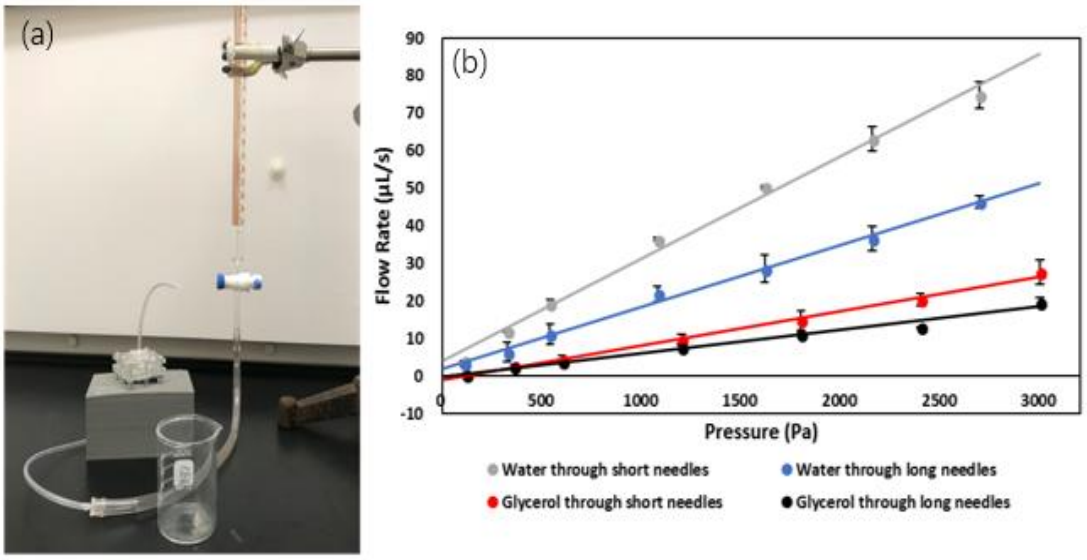

Figure 4.4. (a) A picture of the setup for the experiment of liquid transport through the SED. (b) The flow rates of water and glycerol solutions through short and long microneedles driven by different pressures.

To get an insight into these results, the Hagen-Poiseuille equation should be employed, which can be used to calculate the volumetric flow rate of Newtonian fluid that flow laminarly through a cylindrical pipe with a constant radius R.[103] This equation is expressed as follows:

$$Q = \frac{\pi \Delta P R^4}{8 \mu L} \qquad 4.2$$

where ΔP is the pressure drop between the ends of the tube, μ is the dynamic viscosity of the liquid and L is the length of the tube.[103] When ΔP and μ is constant, Q is inversely proportional to L, meaning that shorter needles can lead to a faster transport rate. Under a certain ΔP, when the needle length L is constant, Q is inversely proportional to μ. The liquid with a lower viscosity will have a higher flow rate. Our results are consistent with the Hagen-Poiseuille law.

Based on the two plots about the transport rates of the glycerol solution in Figure 4.4b, one could estimate the pressure difference across the microneedles that is required to extract a

desired volume of body fluid within a desired duration of time. For example, to fill the sample-collection chamber of the SED (volume: ~300 μL) with blood in 15 s, when using the transdermal patches with short and long needles, the pressure in the chamber should be 2.3 and 3.2 kPa smaller than the pressure inside the human skin, respectively. In fact, the capillary pressure of an adult is normally 2.2-2.4 kPa higher than the atmospheric pressure.[104] Therefore, even the collection chamber is not manually depressurized, body fluid should be able to be extracted out automatically and quickly through both types of microneedles.

4.6 Lactate Detection in the Device

After that the sealing of the SED was confirmed to be reliable, and the mass transport experiments were successfully done, the simultaneous sample collection and detection using the membrane sensors were investigated.

4.6.1 Materials and Methods

First of all, a membrane sensor was adhered to the back of the transdermal patch by epoxy and they were assembled inside the SED. Then, the sensor was electrically wired to the electrochemical workstation. A picture of this setup is presented in Figure 4.3f.

Before lactate detection, 2 mL of 1× PBS was pumped into the device by a syringe and several cycles of DPV was performed to activate the electrodes. During the DPV scans, both the bottom and upper tubes were closed to keep the liquid inside the device. After the scans were completed, the liquid was drained out of the device from the bottom tube. For lactate detection, about 1.5 mL testing sample was pumped into the device each time. The upper chamber was bound to be filled with the testing sample. PBS with increasing concentrations of lactate was pumped into the device and drained out in sequence. One DPV gram acquired by the membrane sensor was generated for each concentration of lactate. Some important parameters of DPV used were as follows: the potential decreased from -0.1 V to -0.8 V; the pulse width, sample width, pulse period were 0.1 s, 0.01 s and 0.8 s, respectively.

4.6.2 Results and Discussion

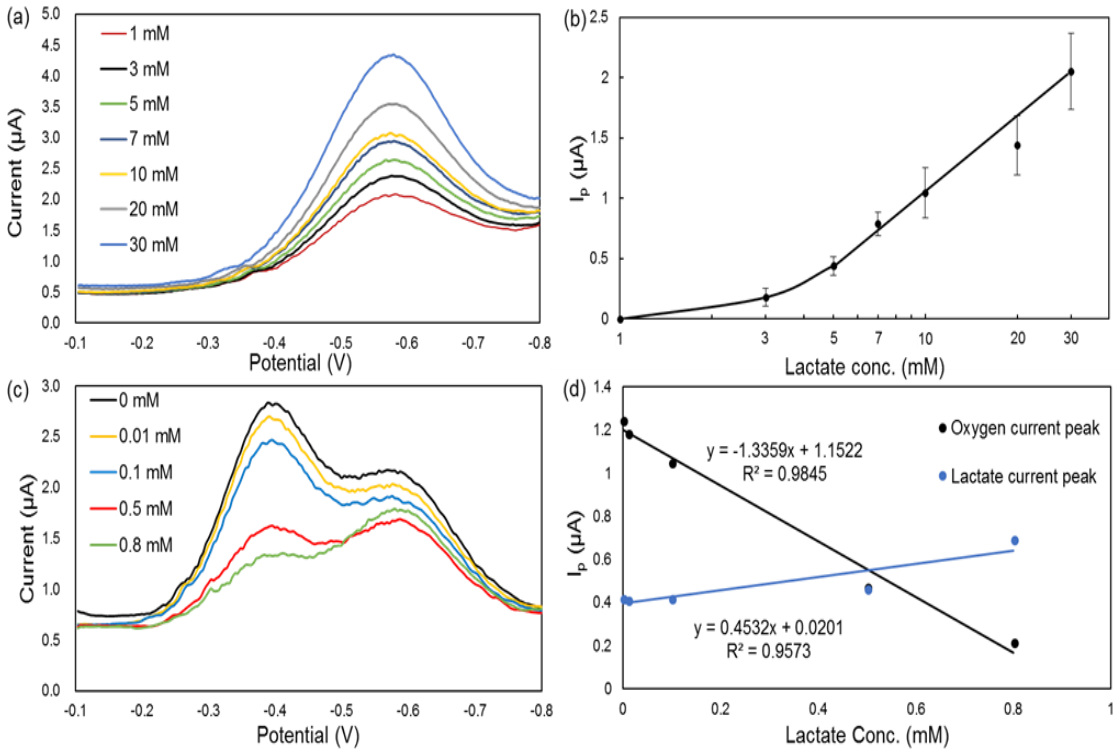

Figure 4.5. (a) The DPV grams of one membrane sensor immersed in PBS with different lactate concentrations in the SED. (b) The calibration curve of the membrane sensors in PBS in the device which shows the change of I_p over lactate concentration on a semi-logarithmic scale. (c) The DPV grams of one membrane sensor immersed in PBS with low lactate concentrations in the SED. (d) The relationship between the I_p of both oxygen and lactate peaks detected by the membrane sensor and the corresponding lactate concentration.

All the results of lactate detection by the membrane sensor inside the SED are presented in Figure 4.5. Figure 4.5a shows the DPV grams of one membrane sensor for various lactate concentrations in PBS. The DPV spectra in Figure 4.5a are consistent with the CV signals collected from the membrane sensors that detected lactate in beakers. There is a defined peak at about -0.6 V which represents the reduction of H_2O_2. Although the peak position varies a little compared to that in the CV grams, this peak grows with the increasing lactate concentration. Again, to plot one calibration curve for all three membrane sensors, baseline correction was done by subtracting the I_p of 1 mM lactate from other I_p. In Figure 4.5b, the calibration curve is plotted in semi-log scale. As can be seen from the calibration curve, the membrane sensors that are placed inside the SED retained the dynamic response range from 4 to 30 mM. This result confirms that the membrane sensor can be assembled into a transdermal

device and reliably detect lactate in a small amount of sample.

Using DPV, it is possible to inquire into the responses of the membrane sensors to lactate concentrations lower than 1 mM, where an additional peak is observed close to the H_2O_2 peak. As can be seen from Figure 4.5c, there is an extra peak at -0.4 V when very low lactate concentrations are detected. This peak drops evidently when the lactate concentration increases. It is identified as the reduction peak of O_2. According to the principle of lactate detection (Equation 1.1 & 1.3), O_2 is consumed to produce H_2O_2 and the reduction of H_2O_2 generates no O_2. Thus, O_2 level decreases as the lactate concentration increases. To further verify, the DPV grams of PBS were recorded before and after nitrogen was bubbled through the solution. The peak at -0.4 V declined sharply after nitrogen bubbling to reduce oxygen.

Figure 4.5d presents how the I_p of the O_2 and H_2O_2 peaks vary with the lactate concentration. Based on the specific values of the slopes of the two plots, we can see that the decline of O_2 signal is 3 times faster than the increase of H_2O_2 signal. According to Equation 1.1 and 1.3, O_2 and H_2O_2 are consumed and produced at the same rate since their stoichiometric ratio is 1. On the WE, the reduction of H_2O_2 and O_2 yields 2 and 4 electrons, respectively. To sum up, the decline of O_2 peak should be 2 times faster than the increase of H_2O_2 peak in theory. In the experiments, the H_2O_2 peak grows slower than expected. The reason is that O_2 reduction can go through either a 4-electron direct pathway, or a succession of two bi-electronic steps which involves H_2O_2 as an intermediate species. In another word, H_2O_2 is generated not only by lactate oxidation but also by O_2 reduction. This also explains why there is a H_2O_2 peak when no lactate presents in the solution. When there is lactate, its oxidation contributes to a larger H_2O_2-reduction I_p. However, since O_2 is consumed the H_2O_2 current caused by O_2 reduction gets smaller. To compensate the loss of current, the H_2O_2 peak is unable to increase at the expected rate.

4.7 Stability of the Membrane Sensor

The results of the previous section also demonstrated the short-term stability of the membrane sensor in the device. To be more comprehensive, the relative long-term stability of

the membrane sensor in a few hours, was investigated.

Before the stability test, 30 mL of 7 mM lactate solution was prepared in 1× PBS. A membrane sensor was assembled into the SED and activated by several CV scans in 1× PBS. The pure PBS was then drained out from the bottom tube, 2 mL of 7 mM lactate solution was pumped into the device using s syringe and the tubes of the device were closed. After the electrodes were immersed in the solution and a quiet time of 10 s, one cycle of CV was applied. The lactate solution was kept inside the device until 5 min later so that the electrodes were constantly immersed in liquid. After 5 min, the old solution was drained out, 2 mL of fresh 7 mM lactate solution was pumped into the device and CV was scanned after the quiet time. Then, this procedure was repeated 10 times, at 15 min, 30 min, 1 h, 2 h, 3 h, 4 h, 5 h, 6 h, 7 h, and 8 h after the first CV test. During the eight hours of the stability test, the membrane sensor was constantly immersed in the lactate solution.

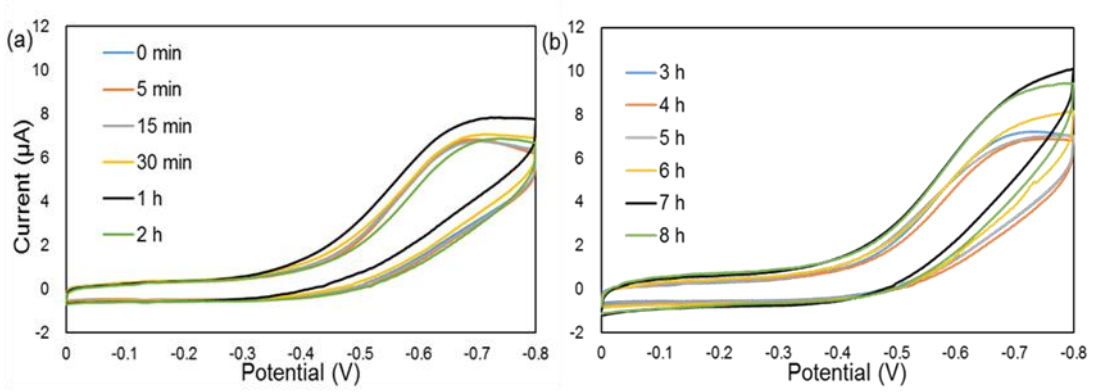

Figure 4.6. The CV grams of one membrane sensor after being constantly immersed in PBS for a certain time: (a) 0 min to 2 h and (b) 3 h to 8 h. (scan rate: 0.05V/s)

The CV grams of the membrane sensor during the stability test are shown in Figure 4.6. The shape of the CV gram remained almost unchanged during the first five hours although there were some slight variations in terms of the value and position of I_p. After 5 h, the shape of the CV grams clearly altered, and the peak height started to significantly increase. Although the CV gram ends at -0.8 V, it appeared that the H_2O_2 peak kept shifting towards the more negative potential side.

To conclude, the membrane sensor can remain relatively stable inside the SED for 5

hours. The fading of the solid-state Ag/AgCl electrode likely caused most of the sensor instability. Over time, the enzyme immobilizing matrix swelled a bit. However, enzyme was successfully retained on the WE for 8 hours since H_2O_2 peak was always observed. If the membrane sensor is immersed in PBS longer, the enzyme matrix can detach from the WE and even dissolve into the solution.

4.8 Lactate Detection in Real Samples

After we confirmed that our lactate membrane sensor was sensitive to lactate concentrations in 1× PBS, we wanted to test it in real body fluid samples. Two types of real samples, human plasma and whole blood, were purchased from BioIVT. Human plasma was frozen at -20 °C, thawed at 37 °C in a water bath, and used at room temperature. Human whole blood was stored at 4 °C, used at room temperature, and disposed after two weeks of storage.

4.8.1 Lactate Detection in Human Plasma

The lactate concentration in pure plasma was unknown. The test samples were prepared according to the various volume ratios between the pure plasma and highly concentrated lactate solution listed in the table in Appendix A. The lactate detection in human plasma was performed in the SED. All procedures, including the electrode activation and the sample detections were the same as stated in Section 4.6.1. In terms of DPV, the same settings were used.

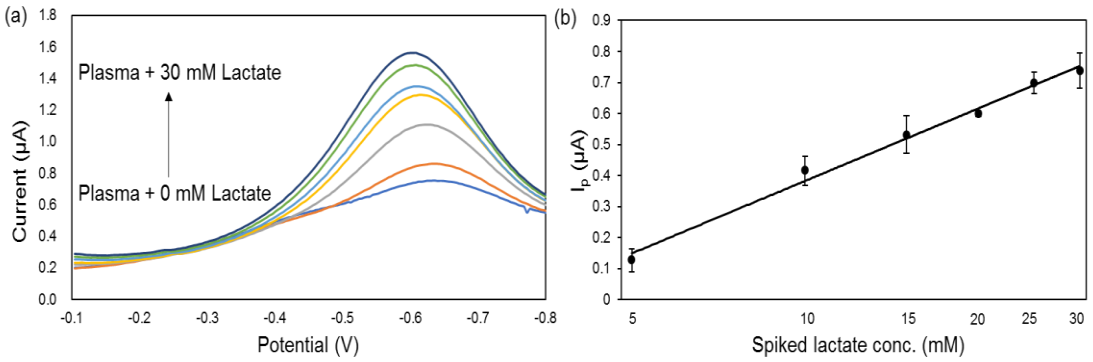

Figure 4.7. (a) The DPV grams of one membrane sensor immersed in human blood plasma with various lactate concentrations in the SED. (b) The calibration curve of the membrane sensors in plasma in the SED which shows the change of I_p over lactate concentration on a semi-logarithmic scale.

The results of lactate detection in human plasma are presented in Figure 4.7. It is clear that in Figure 4.7a, the peak at about -0.6 V elevates as the lactate concentration goes up. To plot the calibration curve of these membrane sensors, the I_p of pure plasma are subtracted from the signals as background correction. In a semi-log scale, as the spiked lactate concentration rises from 5 to 30 mM, I_p increases linearly. Considering the normal lactate level in human body stated before (0.5-2 mM), the dynamic response range of the membrane sensors in plasma is 5.5/7 to 30.5/32 mM, which is similar to the dynamic detection range of the membrane sensors in 1× PBS. This result demonstrates that the membrane sensors can generate stable and reliable signals in response to the lactate concentration in human plasma.

When detecting lactate in 1× PBS, the oxygen peak vanished after 1 mM. However, in Figure 4.7a, there are two peaks in the two nethermost grams, one at -0.4 V which is defined as the oxygen peak as discussed previously and the other at -0.6 V which is the H_2O_2 peak. In another word, oxygen interfering is more pronounced in human plasma compared to that in PBS.

4.8.2 Lactate Detection in Human Whole Blood

The lactate detection in whole blood was conducted in the SED, and all the experimental procedures and settings of DPV were the same as introduced before. The testing solutions were prepared according to the table in Appendix A.

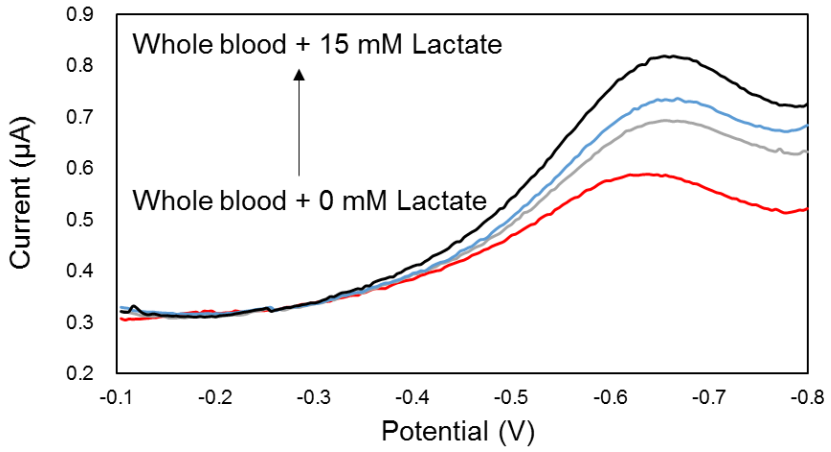

Figure 4.8. The DPV grams of one membrane sensor immersed in human whole blood with various lactate concentrations in the SED.

Using the membrane sensors to detect lactate in human whole blood turns out to be more challenging. Although this experiment has been repeated many times, the set of DPV grams in Figure 4.8 is the only set of data where the H_2O_2 peak does increase with the lactate concentration. Moreover, in this case, when the spiked lactate concentration became larger than 15 mM, the H_2O_2 peak stopped increasing. Other trials provided more disordered results: when the lactate concentration was increased, the H_2O_2 peak could decrease or stay the same.

There are two drawbacks of using the membrane sensors to detect lactate in whole blood: 1) the linear detection range is likely to be narrower; 2) the sensors cannot produce repeatable data. Since there are a large number of cells in whole blood, the blood cells are suspected to significantly disturb the membrane sensors. During lactate detection, cells could hinder the oxygen and lactate molecules from approaching the WE surface. After the first scan of DPV and the membrane sensors were taken out of the blood sample, it was observed that some blood residue remained on the surface of the enzyme matrix or even inside it and could not be rinsed away. It is possible that some reactions or interactions had taken place between the cells and the enzyme matrix during the DPV scan. After that, the enzyme matrix might have been affected and could not function normally. Since the membrane sensors cannot be used in whole blood for multiple times, it is impossible to generate a calibration curve. However, a single DPV scan of the sensor in blood is considered to be reliable.

4.8.3 Comparisons among PBS, Plasma and Blood

To understand how the electrolyte solution affects the signal generated by the membrane sensors, the DPV grams of 10 mM lactate were generated in 2 mL 1× PBS, human plasma and whole blood in sequence in a beaker by the same membrane sensor. This membrane sensor was tested in one solution, fully rinsed by Milli-Q water, dabbed to dry, and then tested in the others. Blood was the last one to be tested since the membrane sensor became unreliable after being used in blood. This procedure was then repeated using other two membrane sensors.

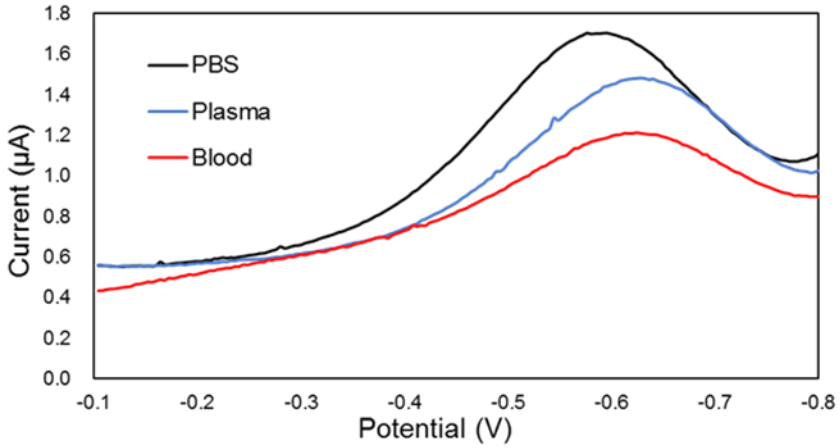

Figure 4.9. The DPV grams of one membrane sensor in 2 mL 1× PBS, human plasma and whole blood that were spiked with 10 mM lactate.

One set of the DPV grams is presented in Figure 4.9. Firstly, it is obvious that although the lactate concentrations in three sample solutions are the same, the three I_p values produced by the same membrane sensor differ from each other. The peak with the maximum height appears in 1×PBS while the peak in blood is the smallest one. To be more precise, the absolute values of I_p of 10 mM lactate in 1× PBS, plasma and blood are listed in Table 4.2. To explain why the I_p of 10 mM lactate varies in the three types of electrolyte solutions, the properties of these solutions should be discussed. Human whole blood is composed of red cells, white cells, platelets and plasma. There are some proteins in plasma while there are only ions in PBS. When they are used as the electrolyte solution of an electrochemical cell, their viscosity is the most concerned parameter.

I_p of a CV gram is inversely proportional to the square root of the viscosity of the electrolyte solution. According to the Equation 3.1 and 3.2, I_p is always proportional to the square root of D, the diffusion constant of the reactant. According to the Stokes-Einstein equation, D is inversely proportional to the viscosity of the medium (η), which is the electrolyte solution in our case, as shown below:[105]

$$D = \frac{K_B T}{6\pi\eta r} \qquad 4.3$$

where K_B is Boltzmann's constant, T is absolute temperature the and r is the radius of the reactant if considering it as a spherical particle.

The conductivity of the electrolyte solution could alter the signal as well. There is no parameter in both Equation 3.1 and 3.2 that is directly related to the conductivity, since the equations consider the electrolyte solution to be ideal, which means, highly conductive. The large number of free ions in the electrolyte solution ensure the instant compensation of the charge created by the electron transfer between the electrode and the analyte.[106] They also help prevent the migration of the analyte.[106] When the electrolyte solution is not conductive enough, the charge compensation might become inefficient and the negative WE would repel the negatively charged lactate molecules, leading to the decrease of the I_p.

The dynamic viscosity values of 1× PBS, human plasma and whole blood, were collected from the literature.[107–109] Their conductivities were determined in the lab using the conductivity meter from VWR at 25 ℃. All these values are summarized in the following table:

	1× PBS	Plasma	Blood
Viscosity at 37 ℃ (cP)	0.7	1.2	4.4
Conductivity at 25 ℃ (S/m)	1.32	1.02	0.51
I_p of 10 mM Lactate (μA)	0.728 (±0.076)	0.589 (±0.140)	0.399 (±0.123)

Table 4.2. The viscosity and conductivity values of 1× PBS, human plasma and whole blood.[107–109] The values of I_p generated by the membrane sensors in these three sample solutions that were spiked with 10 mM lactate.

As shown in Table 4.2, blood has the highest dynamic viscosity which is about 6.3 and 3.7 times more than that of 1× PBS and plasma, respectively. Meanwhile, 1× PBS has the largest conductivity, which is about 1.3 and 2.6 times more than that of plasma and blood. According to the effects of electrolyte conductivity and viscosity on I_p, the membrane sensors should generate the largest I_p in 1× PBS, and the smallest I_p in blood. Our experimental result is consistent with the theoretical deduction.

The second difference among the three DPV grams is the peak potential. The peak

potentials in both plasma and blood are more negative than that in PBS. This might indicate that plasma and blood have similar Cl^- concentration, while both have a less Cl^- concentration than 1× PBS. Difference in viscosity (i.e. mass transport of Cl^-) can also lead to peak shift.

Chapter 5. Glucose Biosensor

5.1 Introduction of Glucose Monitoring

As stated previously, glucose is another essential analyte in the human body. In fact, since diabetes mellitus affects a large population all over the world, glucose biosensors command over 80 % of the biosensor market.[110] To realize the daily and convenient monitoring of glucose for diabetics, the glucose biosensor was firstly commercialized by Yellow Springs Instrument Company (YSI; Yellow Springs, Ohio, USA) in 1975.[91] Since then, glucose biosensors have been the greatest interest of the researchers who investigate biosensors. As a result, in this work, we simply replaced LOD with glucose oxidase (GOD) to see if our membrane sensor could detect glucose.

The same as lactate, glucose has two forms, D-glucose and L-glucose. The glucose discussed in this work is D-glucose since glucose naturally exist in this form. Glucose can present in two structures, the chain form and the ring form, and these two structures are presented in the following figure:[111]

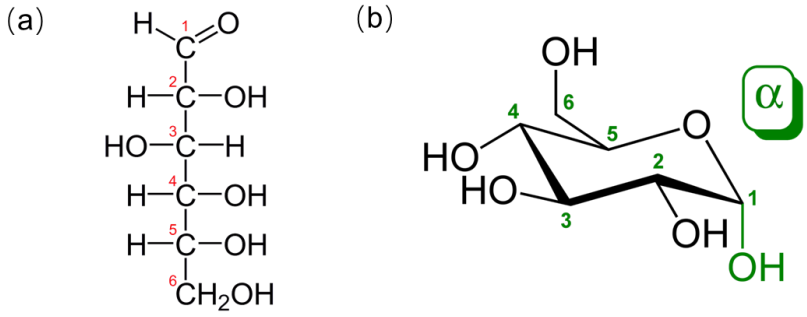

Figure 5.1. (a) The chain and (b) the ring form of glucose.[111]

The principle of the glucose detection in this work was almost the same as the lactate detection. Two consequent reactions take place on the surface of the WE:

$$Glucose + O_2 \xrightarrow{GOD} Gluconic\ acid + H_2O_2 \quad (5.1)$$

$$H_2O_2 + 2H^+ + 2e^- \rightarrow 2H_2O \quad (5.2)$$

Firstly, by the catalyzation of glucose oxidase, glucose is oxidized and H_2O_2 is produced. H_2O_2 is then reduced because of the potential applied onto the WE and the current signal that represent the concentration of glucose can be detected by the membrane sensor.

5.2 Glucose Detection in Plasma

GOD lyophilized powder and D-(+)-glucose powder were purchased from Sigma Aldrich. 20 mg/ml GOD solution was prepared with 1× PBS. The immobilization of GOD on the WE, with the assistance of GA and BSA, followed the same procedure as the immobilization of LOD. Sample solutions for the glucose detection in plasma were prepared according to the table in Appendix B. The membrane sensors were placed inside the SED for the glucose detection. All the experimental procedures and the settings of DPV stayed unchanged as introduced before.

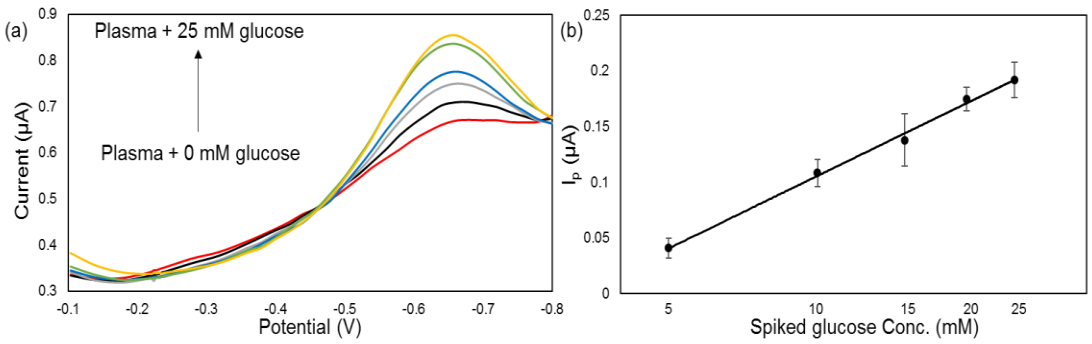

Figure 5.2. (a) The DPV grams of one membrane sensor immersed in human blood plasma with different glucose concentrations in the SED. (b) The calibration curve of the membrane sensors in plasma in the device which shows the change of I_p over glucose concentration on a semi-logarithmic scale.

Judging from the results shown in Figure 5.2, our membrane sensors are able to detect glucose in human plasma. As can be seen from the DPV grams in Figure 5.1a, stable signals are recorded by the membrane sensor. There is a defined peak at about -0.65 V, which results from the reduction of H_2O_2. This peak rises as the glucose concentration in the plasma is elevated. The calibration curve is shown in Figure 5.1b. As the spiked glucose concentration increased from 5 mM to 25 mM, the membrane sensors provide a linear response in terms of the logarithmic concentration values. The normal glucose level in the human whole blood is

generally higher than that of lactate, which is 3.9-6.2 mM at fasting state and 3.9-7.8 mM at 2 h after meal.[112] If the initial glucose concentration in human plasma is assumed to be 5 mM, our membrane sensors would have a dynamic response range towards the glucose concentration in human plasma from 10 to 30 mM.

For both lactate and glucose detections, although I_p increases with the analyte concentration, the absolute value of I_p differs for two systems. When the concentration of the analyte in human plasma increases from 5 mM to 30 mM, the lactate signal rises by about 0.7 μA while the glucose signal rises by only 0.2 μA. In this case, the efficiency difference between the two enzymatic reactions is likely to lead to the different growing rates of I_p. According to the information provided by the vendors, the GOD activity is 100-250 units/mg and its molecular weight is 160 kDa; the LOD activity is 20-60 units/mg and its molecular weight is 80 kDa. Since the masses of the two enzymes on the WE are the same, the molar ratio between GOD and LOD is 1:2. The molar activity of the GOD and LOD can be calculated as 1.6×10^{10}- 4×10^{11} units/mol and 1.6×10^{9}- 4.8×10^{9} units/mol. As a result, if both GOD and LOD are ideally immobilized and preserved on the electrode surface, glucose oxidation will be more efficient than lactate oxidation. This cannot explain our results, but it is possible that the amount of active LOD in this particular immobilizing matrix is higher than that of active GOD. The other reasonable explanation is the different diffusion rates of glucose and lactate molecules in human plasma. Generally speaking, the diffusion rate of a particle is inversely proportional to its molecular weight. Glucose is 180.16 g/mol and lactate has a molecular weight of 89.08 g/mol. As a result, lactate is likely to diffuse faster than glucose in human plasma and generate a stronger signal. According to our results, the rate-determining step on the WE surface is the mass transport of the analytes instead of the enzymatic reaction.

Chapter 6. Summary and Future Work

Lactate is an essential health indicator and its precise monitoring is required. To simplify the process of the lactate monitoring in the human body, capillary blood and ISF, instead of whole blood, can be extracted as the sample to be detected. The extraction of the desired body fluids can be accomplished by microneedles. After the sample collection, electrochemical biosensors provide a simple and reliable method to detect the level of lactate. In this thesis, a lactate biosensor was developed and combined with a transdermal microneedle patch to present the whole process of lactate monitoring in the human body, from the sample collection to its detection.

The fabrication of the lactate biosensor was presented in detail in Chapter 2. This biosensor consisted of three electrodes, which was RE, WE and CE, respectively. The electrodes were made of gold, which were deposited on vinyl paper by EB-PVD. To fabricate the RE, which was a solid-state Ag/AgCl electrode, the electrochemical deposition of silver and the partial chlorination of silver were performed. On the surface of WE, LOD was immobilized by GA in company with BSA. In this way, the enzyme activity was kept and the diffusion of LOD to the sample solution was prevented.

In Chapter 3, the principles of CV and DPV, which were the approaches used to characterize the lactate biosensor, were introduced. The relation between the peak in CV that and the lactate concentration was determined by a standard electrode system. After that, the fabricated lactate membrane biosensors were tested in PBS with various lactate concentrations. The CV grams of the biosensors also presented the targeted peak and a dynamic detection range of 4 to 30 mM was acquired.

In Chapter 4, the fabrication and purpose of the SED were presented. The transdermal patch and the lactate biosensor were assembled together inside the SED. The sample to be detected was pumped into the device through the microneedles to immerse the biosensor. Inside the device, although there was a small amount of test solution and a large pressure applied to the lactate sensor, it could function the same as it did in the beakers. Real body

fluid samples, human plasma and whole blood, were used to test the lactate biosensor. It turned out that the sensor could generate reliable signals in plasma while not in whole blood.

In Chapter 5, a glucose biosensor was fabricated by simply replacing the LOD on the WE surface by GOD. This glucose biosensor could sensitively response to the glucose concentration in human plasma from 10 to 30 mM when assembled inside the SED.

The lactate biosensor developed and tested in this thesis was based on a simple configuration. To realize the practical use of this membrane biosensor, it is required to be modified and improved in many aspects.

First of all, it must be able to conduct detection in whole blood samples. The most direct solution that we proposed is to place a filter between the transdermal patch and the lactate biosensor. This filter should be able to filter out the blood cells and thus only plasma can reach the sensor. However, common filter membranes, including those made of poly(ether sulfones), polycarbonate, glass fiber and cellulose, were unable to meet our requirement. When they were used to separate blood cells and plasma, cells could be easily broken if a pressure was applied to push the liquid through, or the pores could be clogged by cells and nothing could come out at the other side if no pressure was applied. Up to now, one product, called blood separator, is the most potential candidate. It is a thick and hydrophilic paper with a highly porous structure. When blood is dropped onto it, blood can be absorbed and migrates inside the paper. This product separates plasma from whole blood since plasma travels further than the cells inside it. In the SED, we made another chamber for the blood separator, which was located between the transdermal patch and the lactate biosensor (a picture of the set-up is shown in Appendix C). In this chamber, the blood separator was rolled like a roll paper. A syringe pump was used to pump about 1.5 mL of whole blood into the device at a constant and slow speed. After a few minutes, we observed plasma (with some blood cells) in the upper chamber whose volume was adequate for the biosensor to detect lactate. Preliminary results demonstrated the feasibility of using the blood separator to collect a relatively large volume of plasma from whole blood, but further modifications should be made to minimize

the volume of whole blood required.

Since we want the membrane sensor to detect the lactate level in human body every 5 minutes for at least 8 hours, the stability of the sensor should be improved, and the sensor lifetime requires to be elongated.

The stability of the reference electrode greatly influences the sensor lifetime. As discussed before, the solid-state Ag/AgCl electrode fabricated in this thesis could not keep stable for a long time. Covering the electrode with a gel rich in Cl^- as mentioned in section 2.2.1 is worth trying. Other methods of making the solid-state Ag/AgCl electrode are possible to generate more stale electrodes. More literature research about other types of solid-state reference electrodes is required to find a solid-state reference electrode that is intrinsically more stable than the solid-state Ag/AgCl electrode.

Besides the reference electrode, the enzyme electrode is an essential factor that affects not only the stability of the biosensor but also the sensitivity of the signal. Some nanostructures could be introduced onto the surface of the WE; For example, a silver layer with nano-structures could be generated on the WE surface. In this way, the surface area of the electrode will be enlarged sharply; more enzymes could be immobilized close to the electrode and this kind of structure is beneficial to keep the enzymes active. In the enzyme immobilizing matrix, more nanomaterials could be added, such as carbon nanotubes. Conducting nanomaterials could facilitate the electron transfer within the matrix and enhance the sensitivity of the signal. Other enzyme immobilization methods, such as immobilizing enzymes into hydrogel, are worth trying. To evaluate the efficiency of various enzyme immobilization methods, one can perform two measurements. The first is to quantify the number of proteins that are actually bounded in the matrix. Some well-developed assays, such as Bradford assay, can be used to accurately determine the number of proteins. The number of immobilized proteins can be determined by getting the difference between the numbers of total proteins and unbounded proteins. The second step of evaluation is to quantify the activity of the immobilized enzyme. We can use established colorimetric assays to determine

enzyme activity. For example, for LOD, there is a well-established assay from Sigma-Aldrich to quantify its activity.[113] This assay uses the absorbance of the final product to represent the activity of LOD. The enzymes can be immobilized on the bottom of the wells of a 96-well plates, using the same crosslinking condition for enzyme immobilization on sensor electrodes. Since the enzymes cannot diffuse freely in the solution, it is necessary to make some adaptions to the assay.

References

1. Hao, Y. & Foster, R. Wireless body sensor networks for health-monitoring applications. *Physiological Measurement* (2008).
2. Wang, X., Liu, Z. & Zhang, T. Flexible Sensing Electronics for Wearable/Attachable Health Monitoring. *Small* **13,** (2017).
3. Bandodkar, A. J. & Wang, J. Non-invasive wearable electrochemical sensors: A review. *Trends in Biotechnology* (2014).
4. Patel, S., Park, H., Bonato, P., Chan, L. & Rodgers, M. A review of wearable sensors and systems with application in rehabilitation. *Journal of NeuroEngineering and Rehabilitation* (2012).
5. Tierney, M. J., Tamada, J. A., Potts, R. O., Jovanovic, L. & Garg, S. Clinical evaluation of the GlucoWatch® biographer: A continual, non-invasive glucose monitor for patients with diabetes. in *Biosensors and Bioelectronics* (2001).
6. Yang, Y. L., Chuang, M. C., Lou, S. L. & Wang, J. Thick-film textile-based amperometric sensors and biosensors. *Analyst* (2010).
7. Kim, J. *et al.* Wearable smart sensor systems integrated on soft contact lenses for wireless ocular diagnostics. *Nat. Commun.* (2017).
8. Yeo, W. H. *et al.* Multifunctional epidermal electronics printed directly onto the skin. *Adv. Mater.* (2013).
9. Kabiri Ameri, S. *et al.* Graphene Electronic Tattoo Sensors. *ACS Nano* (2017).
10. Pantelopoulos, A. & Bourbakis, N. G. A survey on wearable sensor-based systems for health monitoring and prognosis. *IEEE Transactions on Systems, Man and Cybernetics Part C: Applications and Reviews* (2010).
11. Takei, K., Honda, W., Harada, S., Arie, T. & Akita, S. Toward flexible and wearable human-interactive health-monitoring devices. *Adv. Healthc. Mater.* **4,** 487–500 (2015).
12. Bandodkar, A. J. *et al.* Tattoo-based potentiometric ion-selective sensors for epidermal pH monitoring. *Analyst* **138,** 123–128 (2013).
13. Bandodkar, A. J. *et al.* Epidermal tattoo potentiometric sodium sensors with wireless signal transduction for continuous non-invasive sweat monitoring. *Biosens. Bioelectron.* **54,** 603–609 (2014).
14. Guinovart, T., Bandodkar, A. J., Windmiller, J. R., Andrade, F. J. & Wang, J. A potentiometric tattoo sensor for monitoring ammonium in sweat. *Analyst* **138,** 7031 (2013).
15. Yang, S. *et al.* 'cut-and-Paste' Manufacture of Multiparametric Epidermal Sensor Systems. *Adv. Mater.* (2015).

16. Gao, W. *et al.* Fully integrated wearable sensor arrays for multiplexed in situ perspiration analysis. *Nature* (2016).
17. Clark, L. C. & Lyons, C. Electrode systems for continuous monitoring in cardiovascular surgery. *Ann. N. Y. Acad. Sci.* **102,** 29–45 (1962).
18. Eggins, B. *Chemical Sensors and Biosensors*. *Chemical Sensors and Biosensors* (2007).
19. Grieshaber, D., MacKenzie, R., Vörös, J. & Reimhult, E. Electrochemical Biosensors - Sensor Principles and Architectures. *Sensors* **8,** 1400–1458 (2008).
20. Scheller, F. W. *et al.* Biosensors: trends and commercialization. *Biosensors* (1985).
21. Singh, M., Verma, N., Garg, A. K. & Redhu, N. Urea biosensors. *Sensors and Actuators, B: Chemical* **134,** 345–351 (2008).
22. Chen, C. *et al.* Recent advances in electrochemical glucose biosensors. *RSC Adv.* **3,** 4473–4491 (2013).
23. Rassaei, L., Olthuis, W., Tsujimura, S., Sudhölter, E. J. R. & Van Den Berg, A. Lactate biosensors: Current status and outlook. *Analytical and Bioanalytical Chemistry* **406,** 123–137 (2014).
24. Mandel, A. & Lusk, G. Lactic acid in intermediary metabolism. *Am. J. Physiol.* **16,** 129–146 (1906).
25. Allen, S. E. & Holm, J. L. Lactate: Physiology and clinical utility. *J. Vet. Emerg. Crit. Care* **18,** 123–132 (2008).
26. Madias, N. E. Lactic acidosis. *Kidney Int.* **29,** 752–774 (1986).
27. Yudkin, J. & Cohen, R. D. The contribution of the kidney to the removal of a lactic acid load under normal and acidotic conditions in the conscious rat. *Clin. Sci. Mol. Med.* (1975).
28. Pyne, D. B., Boston, T., Martin, D. T. & Logan, A. Evaluation of the Lactate Pro blood lactate analyser. *Eur. J. Appl. Physiol.* **82,** 112–116 (2000).
29. Derbyshire, P. J., Barr, H., Davis, F. & Higson, S. P. J. Lactate in human sweat: A critical review of research to the present day. *Journal of Physiological Sciences* **62,** 429–440 (2012).
30. Faude, O., Kindermann, W. & Meyer, T. Lactate threshold concepts: How valid are they? *Sports Medicine* **39,** 469–490 (2009).
31. Mizock, B. A. & Falk, J. L. Lactic acidosis in critical illness. in *Critical Care Medicine* (1992).
32. Tanner, R. K., Fuller, K. L. & Ross, M. L. R. Evaluation of three portable blood lactate analysers: Lactate Pro, Lactate Scout and Lactate Plus. *Eur. J. Appl. Physiol.* **109,** 551–559 (2010).

33. Bonaventura, J. M. *et al.* Reliability and accuracy of six hand-held blood lactate analysers. *J. Sport. Sci. Med.* **14,** 203–214 (2014).
34. Chen, Q. *et al.* Flexible electrochemical biosensors based on graphene nanowalls for the real-time measurement of lactate. *Nanotechnology* **28,** 315501 (2017).
35. Lei, Y. *et al.* A highly sensitive electrochemical biosensor based on zinc oxide nanotetrapods for l-lactic acid detection. *Nanoscale* **4,** 3438–3443 (2012).
36. Hernández-Ibáñez, N. *et al.* Electrochemical lactate biosensor based upon chitosan/carbon nanotubes modified screen-printed graphite electrodes for the determination of lactate in embryonic cell cultures. *Biosens. Bioelectron.* **77,** 1168–1174 (2016).
37. Jia, W. *et al.* Electrochemical tattoo biosensors for real-time noninvasive lactate monitoring in human perspiration. *Anal. Chem.* **85,** 6553–6560 (2013).
38. Pohanka, M. & Republic, C. Electrochemical biosensors – principles and applications. *Methods* (2008).
39. Waleed Shinwari, M. *et al.* Microfabricated reference electrodes and their biosensing applications. *Sensors* (2010).
40. Rassaei, L., Olthuis, W., Tsujimura, S., Sudhölter, E. J. R. & van den Berg, A. Lactate biosensors: current status and outlook. *Anal. Bioanal. Chem.* **406,** 123–137 (2014).
41. D. A. McQuarrie, P. A. Rock, and E. B. G. *General chemistry,4th ed*.
42. Hickey, D. P., Reid, R. C., Milton, R. D. & Minteer, S. D. A self-powered amperometric lactate biosensor based on lactate oxidase immobilized in dimethylferrocene-modified LPEI. *Biosens. Bioelectron.* (2016).
43. Malon, R. S. P., Chua, K. Y., Wicaksono, D. H. B. & Córcoles, E. P. Cotton fabric-based electrochemical device for lactate measurement in saliva. *Analyst* (2014).
44. Menten, L. & Michaelis, M. Kinetics of invertase action. *Biochem Z* **49,** 333–369 (1913).
45. Thomas Shafee. Saturation curve for an enzyme reaction showing the relation between the substrate concentration and reaction rate. (2015). Available at: https://commons.wikimedia.org/wiki/File:Michaelis_Menten_curve_2.svg.
46. Singh, J. & Wolfe, D. E. Review Nano and macro-structured component fabrication by electron beam-physical vapor deposition (EB-PVD). *J. Mater. Sci.* **40,** 1–26 (2005).
47. Singh, J. & Wolfe, D. E. Nanostructured component fabrication by electron beam-physical vapor deposition. in *Journal of Materials Engineering and Performance* (2005).
48. Singh, J., Quli, F., Wolfe, D. E. & Schriempf, J. An Overview: Electron Beam-Physical Vapor Deposition Technology-Present and Future Applications. *Surf. Eng.*

Sci. Technol. I (1999).

49. Wolfe, D. E., Singh, J. & Narasimhan, K. Synthesis and characterization of multilayered TiC/TiB2coatings deposited by ion beam assisted, electron beam-physical vapor deposition (EB-PVD). *Surf. Coatings Technol.* (2003).
50. Sarma, A. K., Vatsyayan, P., Goswami, P. & Minteer, S. D. Recent advances in material science for developing enzyme electrodes. *Biosensors and Bioelectronics* **24,** 2313–2322 (2009).
51. Guo, S., Wen, D., Zhai, Y., Dong, S. & Wang, E. Platinum nanoparticle ensemble-on-graphene hybrid nanosheet: One-pot, rapid synthesis, and used as new electrode material for electrochemical sensing. *ACS Nano* **4,** 3959–3968 (2010).
52. Pingarrón, J. M., Yáñez-Sedeño, P. & González-Cortés, A. Gold nanoparticle-based electrochemical biosensors. *Electrochim. Acta* **53,** 5848–5866 (2008).
53. Zhang, S., Wang, N., Yu, H., Niu, Y. & Sun, C. Covalent attachment of glucose oxidase to an Au electrode modified with gold nanoparticles for use as glucose biosensor. *Bioelectrochemistry* **67,** 15–22 (2005).
54. Shelley D. Minteer. *Microfluidic Techniques: Reviews and Protocols*. (2006).
55. Hamann, C. H., Hamnett, A. & Vielstich, W. *Electrochemistry*. *Wiley-VCH Verlag GmbH & Co. KGaA* (2007).
56. Kim, T. Y., Hong, S. A. & Yang, S. A solid-state thin-film Ag/AgCl reference electrode coated with graphene oxide and its use in a pH sensor. *Sensors (Switzerland)* (2015).
57. Noh, J., Park, S., Boo, H., Kim, H. C. & Chung, T. D. Nanoporous platinum solid-state reference electrode with layer-by-layer polyelectrolyte junction for pH sensing chip. *Lab Chip* (2011).
58. Polk, B. J., Stelzenmuller, A., Mijares, G., MacCrehan, W. & Gaitan, M. Ag/AgCl microelectrodes with improved stability for microfluidics. *Sensors Actuators B Chem.* **114,** 239–247 (2006).
59. Moussy, F. & Harrison, D. J. Prevention of the Rapid Degradation of Subcutaneously Implanted Ag/AgCl Reference Electrodes Using Polymer Coatings. *Anal. Chem.* **66,** 674–679 (1994).
60. Huang, I. Y. & Huang, R. S. Fabrication and characterization of a new planar solid-state reference electrode for ISFET sensors. *Thin Solid Films* (2002).
61. Liao, W. Y. & Chou, T. C. Fabrication of a planar-form screen-printed solid electrolyte modified Ag/AgCl reference electrode for application in a potentiometric biosensor. *Anal. Chem.* (2006).
62. Polk, B. J., Stelzenmuller, A., Mijares, G., MacCrehan, W. & Gaitan, M. Ag/AgCl microelectrodes with improved stability for microfluidics. *Sensors Actuators, B Chem.*

(2006).

63. Cranny, A. W. J. & Atkinson, J. K. Thick film silver – silver chloride reference electrodes. *Solutions* (1998).
64. Suzuki, H., Hiratsuka, A., Sasaki, S. & Karube, I. Problems associated with the thin-film Ag/AgCl reference electrode and a novel structure with improved durability. *Sensors Actuators B Chem.* **46,** 104–113 (1998).
65. Almeida, F. L. *et al.* Fabrication Process of Ag/AgCl Reference Pseudo-Electrode Based on Electrodeposition of Au on Pt Surfaces from Formaldehyde Baths: Chemical Stability and Adherence. in *ECS Transactions* (2009).
66. Sassolas, A., Blum, L. J. & Leca-Bouvier, B. D. Immobilization strategies to develop enzymatic biosensors. *Biotechnology Advances* **30,** 489–511 (2012).
67. Sassolas, A., Blum, L. J. & Leca-Bouvier, B. D. Immobilization strategies to develop enzymatic biosensors. *Biotechnology Advances* (2012).
68. Campàs, M., Bucur, B., Andreescu, S. & Marty, J.-L. *Application of oriented immobilisation to enzyme sensors*. *Curr Top Biotechnol* **1,** (2004).
69. Wang, J. Carbon-nanotube based electrochemical biosensors: A review. *Electroanalysis* **17,** 7–14 (2005).
70. Luo, X., Morrin, A., Killard, A. J. & Smyth, M. R. Application of nanoparticles in electrochemical sensors and biosensors. *Electroanalysis* (2006).
71. Bowes, J. H. & Cater, C. W. The interaction of aldehydes with collagen. *BBA - Protein Struct.* (1968).
72. Habeeb, A. F. S. A. & Hiramoto, R. Reaction of proteins with glutaraldehyde. *Arch. Biochem. Biophys.* (1968).
73. Avrameas, S. & Ternynck, T. The cross-linking of proteins with glutaraldehyde and its use for the preaparation of immunoadsorbernts. *Immunochemistry* (1969).
74. Migneault, I., Dartiguenave, C., Bertrand, M. J. & Waldron, K. C. Glutaraldehyde: Behavior in aqueous solution, reaction with proteins, and application to enzyme crosslinking. *BioTechniques* (2004).
75. Crespilho, F. N. *et al.* A strategy for enzyme immobilization on layer-by-layer dendrimer-gold nanoparticle electrocatalytic membrane incorporating redox mediator. *Electrochem. commun.* (2006).
76. De Luca, S. *et al.* Carbon film electrodes for oxidase-based enzyme sensors in food analysis. in *Talanta* (2005).
77. Fiorito, P. A., Brett, C. M. A. & Córdoba De Torresi, S. I. Polypyrrole/copper hexacyanoferrate hybrid as redox mediator for glucose biosensors. in *Talanta* (2006).
78. Islan, G. A., Martinez, Y. N., Illanes, A. & Castro, G. R. Development of novel

alginate lyase cross-linked aggregates for the oral treatment of cystic fibrosis. *RSC Adv.* (2014).

79. Brownson, D. A. C. & Banks, C. E. *The Handbook of Graphene Electrochemistry*. *The Handbook of Graphene Electrochemistry* (2014).
80. Kissinger, P. T. & Heineman, W. R. Cyclic voltammetry. *J. Chem. Educ.* **60,** 702 (1983).
81. Shrivastava, A. & Gupta, V. B. Methods for the determination of limit of detection and limit of quantitation of the analytical methods. **2,** 21–25 (2011).
82. Mannoor, M. S. *et al.* Graphene-based wireless bacteria detection on tooth enamel. *Nat. Commun.* **3,** 763 (2012).
83. Chu, M. X. *et al.* Soft contact lens biosensor for in situ monitoring of tear glucose as non-invasive blood sugar assessment. *Talanta* **83,** 960–965 (2011).
84. Mishra, R. K., Vinu Mohan, A. M., Soto, F., Chrostowski, R. & Wang, J. A microneedle biosensor for minimally-invasive transdermal detection of nerve agents. *Analyst* **142,** 918–924 (2017).
85. Emaminejad, S. *et al.* Autonomous sweat extraction and analysis applied to cystic fibrosis and glucose monitoring using a fully integrated wearable platform. *Proc. Natl. Acad. Sci.* **114,** 4625–4630 (2017).
86. Sabat, J. *et al.* The use of finger-stick blood to assess lactate in critically ill surgical patients. *Ann. Med. Surg.* **10,** 41–48 (2016).
87. Petersen, L. J. Interstitial lactate levels in human skin at rest and during an oral glucose load: a microdialysis study. *Clin. Physiol.* **19,** 246–250 (1999).
88. Tobin, D. J. Biochemistry of human skin—our brain on the outside. *Chem. Soc. Rev.* **35,** 52–67 (2006).
89. Ventrelli, L., Marsilio Strambini, L. & Barillaro, G. Microneedles for Transdermal Biosensing: Current Picture and Future Direction. *Adv. Healthc. Mater.* **4,** 2606–2640 (2015).
90. Roe, J. N. & Smoller, B. R. Bloodless glucose measurements. *Crit.Rev.Ther.Drug Carr. Syst.* **15,** 199–241 (1998).
91. Setford, S. J. & Newman, J. D. *Enzyme Biosensors*. *Microbial Enzymes and Biotransformations* **17,** (2005).
92. Khanna, P., Strom, J. A., Malone, J. I. & Bhansali, S. Microneedle-Based Automated Therapy for Diabetes Mellitus. *J. Diabetes Sci. Technol.* **2,** 1122–1129 (2008).
93. Prausnitz, M. R. Microneedles for transdermal drug delivery. *Advanced Drug Delivery Reviews* **56,** 581–587 (2004).
94. Henry, S., McAllister, D. V., Allen, M. G. & Prausnitz, M. R. Microfabricated

microneedles: A novel approach to transdermal drug delivery. *J. Pharm. Sci.* **87,** 922–925 (1998).

95. Smart, W. H. & Subramanian, K. The use of silicon microfabrication technology in painless blood glucose monitoring. *Diabetes Technol. Ther.* (2000).
96. Sivamani, R. K., Liepmann, D. & Maibach, H. I. Microneedles and transdermal applications. *Expert Opin. Drug Deliv.* **4,** 19–25 (2007).
97. Matsuda, T. & Mizutani, M. Liquid acrylate-endcapped biodegradable poly(ε-caprolactone-co-trimethylene carbonate). II. Computer-aided stereolithographic microarchitectural surface photoconstructs. *J. Biomed. Mater. Res.* (2002).
98. Park, J. H., Allen, M. G. & Prausnitz, M. R. Biodegradable polymer microneedles: Fabrication, mechanics and transdermal drug delivery. *J. Control. Release* (2005).
99. Miyano, T. *et al.* Sugar micro needles as transdermic drug delivery system. *Biomed. Microdevices* (2005).
100. Park, J. H., Allen, M. G. & Prausnitz, M. R. Polymer microneedles for controlled-release drug delivery. *Pharm. Res.* (2006).
101. Gill, H. S., Denson, D. D., Burris, B. A. & Prausnitz, M. R. Effect of Microneedle Design on Pain in Human Volunteers. *Clin. J. Pain* **24,** 585–594 (2008).
102. Yousif, M. Y., Holdsworth, D. W. & Poepping, T. L. A blood-mimicking fluid for particle image velocimetry with silicone vascular models. *Exp. Fluids* **50,** 769–774 (2011).
103. Kirby, B. J. *Micro- and Nanoscale Fluid Mechanics: Transport in Microfluidic Devices*. *Brian* (2010).
104. Shore, A. C., Sandeman, D. D. & Tooke, J. E. Capillary pressure, pulse pressure amplitude, and pressure waveform in healthy volunteers. *Am. J. Physiol. Circ. Physiol.* **268,** H147–H154 (1995).
105. Kholodenko, A. L. & Douglas, J. F. Generalized Stokes-Einstein equation for spherical particle suspensions. *Phys. Rev. E* (1995).
106. Elgrishi, N. *et al.* A Practical Beginner's Guide to Cyclic Voltammetry. *J. Chem. Educ.* (2017).
107. Soenksen, L. R., Kassis, T., Noh, M., Griffith, L. G. & Trumper, D. L. Closed-loop feedback control for microfluidic systems through automated capacitive fluid height sensing. *Lab Chip* (2018).
108. Késmárky, G., Kenyeres, P., Rábai, M. & Tóth, K. Plasma viscosity: A forgotten variable. in *Clinical Hemorheology and Microcirculation* (2008). doi:10.3233/CH-2008-1088
109. Yousif, M. Y., Holdsworth, D. W. & Poepping, T. L. A blood-mimicking fluid for

particle image velocimetry with silicone vascular models. *Exp. Fluids* (2011).

110. Wang, J. Electrochemical glucose biosensors. in *Electrochemical Sensors, Biosensors and their Biomedical Applications* (2008).
111. Ben & Yikrazuul. D-glucose-chain-2D-Fischer. (2006). Available at: https://commons.wikimedia.org/wiki/File:D-glucose-chain-2D-Fischer.png#/media/File:D-glucose.png.
112. Chen, C. *et al.* Recent advances in electrochemical glucose biosensors: A review. *RSC Advances* (2013).
113. Enzymatic Assay of LACTATE OXIDASE. Available at: https://www.sigmaaldrich.com/content/dam/sigma-aldrich/docs/Sigma/General_Information/2/lactate_oxidase.pdf.

Appendix A

Spiked Lactate Conc. (mM)	Plasma (Whole blood)	0.5 M Lactate Solution	1 M Lactate Solution
Pure plasma	1	0	0
5	1	0.01	0
10	1	0	0.01
15	1	0	0.015
20	1	0	0.02
25	1	0	0.025
30	1	0	0.03

Compositions of the sample solutions for lactate detection in plasma or whole blood. To increase the lactate concentration in the real body fluid, highly concentrated (0.5 M or 1 M) lactate solution was added based on the listed volume ratio.

Spiked Glucose Conc. (mM)	Human Plasma	0.5 M Glucose Solution	1 M Glucose Solution
Pure plasma	1	0	0
5	1	0.01	0
10	1	0	0.0.1
15	1	0	0.015
20	1	0	0.02
25	1	0	0.025

Appendix B

Compositions of the sample solutions for glucose detection in plasma. To increase the glucose concentration in pure plasma, 0.5 or 1 M glucose solution was added to the pure plasma based on the listed volume ratio.

Appendix C

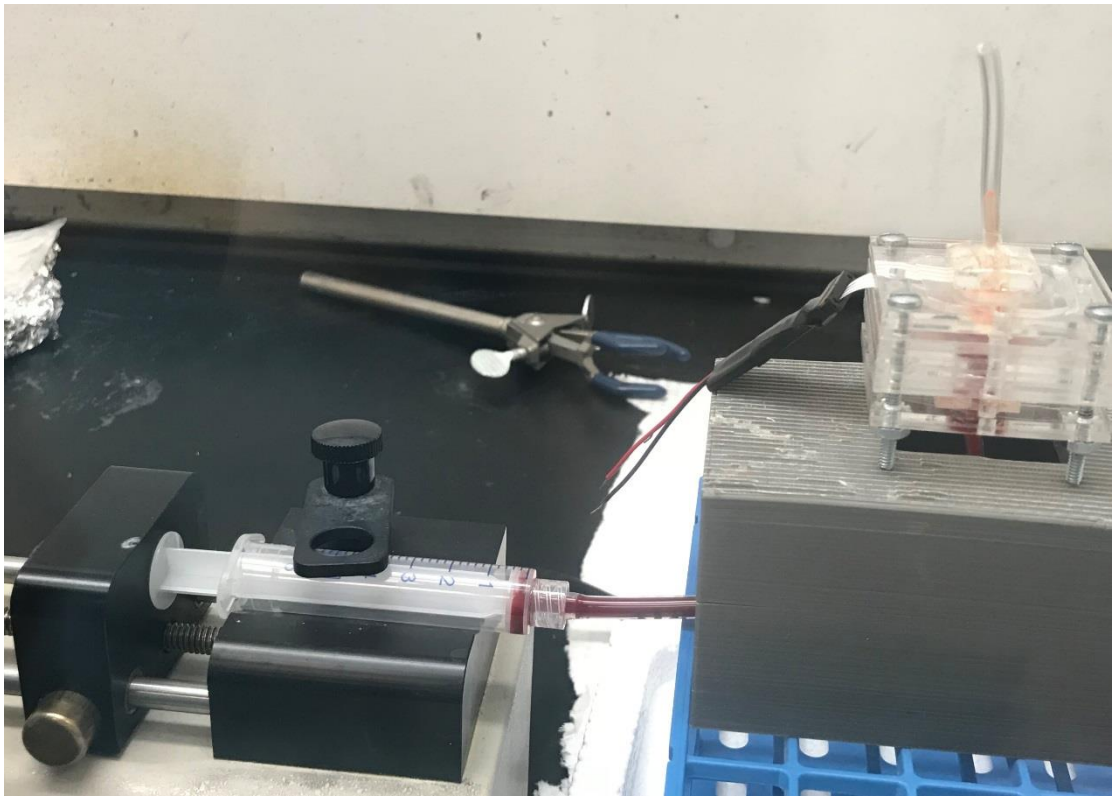

A picture of the set-up to separate plasma from whole blood.